AGU PUBLICATIONS

JGR

Journal of Geophysical Research: Oceans

RESEARCH ARTICLE

10.1002/2017JC013288

Biogeochemical Impact of Snow Cover and Cyclonic Intrusions on the Winter Weddell Sea Ice Pack

J.-L. Tison[1], S. Schwegmann[2], G. Dieckmann[2], J.-M. Rintala[3], H. Meyer[2], S. Moreau[4], M. Vancoppenolle[5], D. Nomura[6,7], S. Engberg[3], L. J. Blomster[3], S. Hendricks[2], C. Uhlig[2], A.-M. Luhtanen[8,9,10], J. de Jong[11], J. Janssens[4,12,13], G. Carnat[1], J. Zhou[1,14], and B. Delille[14]

[1]Laboratoire de Glaciologie, Department of Geosciences, Environment and Society (DGES) CP 160/03, Université Libre de Bruxelles, Brussels, Belgium, [2]Alfred Wegener Institute, Helmholz Zentrum für Polar und Meeresforschung, Bremerhaven, Germany, [3]Department of Environmental Science, University of Helsinki, Helsinki, Finland, [4]Institute for Marine and Antarctic Studies, University of Tasmania, Hobart, TA, Australia, [5]Sorbonne Universités (UPMC Paris 6), LOCEAN-IPSL, CNRS/IRD/MNHN, Paris, France, [6]Faculty of Fisheries Sciences, Hokkaido University, Hokkaido, Japan, [7]Arctic Research Center, Hokkaido University, Hokkaido, Japan, [8]Marine Research Centre, Finnish Environment Institute, Helsinki, Finland, [9]Department of Biosciences, University of Helsinki, Helsinki, Finland, [10]Tvärminne Zoological Station, University of Helsinki, Hanko, Finland, [11]G-Time Laboratory (Geochemistry tracing by Isotopes, Minerals and Elements), Department of Geosciences, Environment and Society (DGES) CP 160/02, Université Libre de Bruxelles, Brussels, Belgium, [12]Antarctic Climate and Ecosystems Cooperative Research Centre, University of Tasmania, Hobart, TAS, Australia, [13]Australian Antarctic Division, Department of the Environment and Energy, Kingston, TAS, Australia, [14]Chemical Oceanography Unit (COU), Université de Liège, Liège, Belgium

Key Points:
- Winter Weddell Sea pack ice (Antarctica) remains warm and permeable due to large snow depth and frequent occurrence of warm cyclonic events
- These conditions trigger brine dynamics and associated sea ice biogeochemical processes
- Of the limited number of winter Weddell Sea pack ice studies (3), this one reveals higher snow depth, negative freeboard, and higher Chl-*a*

Correspondence to:
J.-L. Tison,
jtison@ulb.ac.be

Citation:
Tison, J.-L., Schwegmann, S., Dieckmann, G., Rintala, J.-M., Meyer, H., Moreau, S., . . . Delille, B. (2017). Biogeochemical impact of snow cover and cyclonic intrusions on the winter Weddell Sea ice pack. *Journal of Geophysical Research: Oceans*, *122*, 9548–9571. https://doi.org/10.1002/2017JC013288

Received 21 JUL 2017
Accepted 20 OCT 2017
Accepted article online 25 OCT 2017
Published online 8 DEC 2017
Corrected 29 MAR 2018

This article was corrected on 29 MAR 2018. See the end of the full text for details.

Abstract Sea ice is a dynamic biogeochemical reactor and a double interface actively interacting with both the atmosphere and the ocean. However, proper understanding of its annual impact on exchanges, and therefore potentially on the climate, notably suffer from the paucity of autumnal and winter data sets. Here we present the results of physical and biogeochemical investigations on winter Antarctic pack ice in the Weddell Sea (R. V. Polarstern AWECS cruise, June–August 2013) which are compared with those from two similar studies conducted in the area in 1986 and 1992. The winter 2013 was characterized by a warm sea ice cover due to the combined effects of deep snow and frequent warm cyclones events penetrating southward from the open Southern Ocean. These conditions were favorable to high ice permeability and cyclic events of brine movements within the sea ice cover (brine tubes), favoring relatively high chlorophyll-a (Chl-*a*) concentrations. We discuss the timing of this algal activity showing that arguments can be presented in favor of continued activity during the winter due to the specific physical conditions. Large-scale sea ice model simulations also suggest a context of increasingly deep snow, warm ice, and large brine fractions across the three observational years, despite the fact that the model is forced with a snowfall climatology. This lends support to the claim that more severe Antarctic sea ice conditions, characterized by a longer ice season, thicker, and more concentrated ice are sufficient to increase the snow depth and, somehow counterintuitively, to warm the ice.

1. Introduction

Almost 10% of the ocean is covered by sea ice at least once a year (calculated from Fetterer et al., 2016, updated daily). Sea ice high surface albedo and impact on polar water masses stratification and atmosphere-ocean heat and moisture exchanges (e.g., Dieckmann & Hellmer, 2010)) are recognized as important to the large-scale climate system. Sea ice also plays a key role in the polar marine ecosystem, hosting microbial communities at various depth levels throughout the year (e.g., Arrigo et al., 2010, 2014; Arrigo & Thomas, 2004; Horner et al., 1992; Lizotte, 2001; Thomas & Dieckmann, 2002). These sympagic organisms have a distinct life cycle within the ice, but they have also been shown to trigger phytoplankton blooms at retreating sea ice margins during the summer (Smith & Nelson, 1986). In-ice and underice algae communities contribute to the cycling of carbon and other major elements in polar seas, and support higher trophic level populations (e.g., krill populations, Bluhm et al., 2010; Flores et al., 2012; Leu et al., 2011).

Sea ice can be seen as a dynamic biogeochemical reactor and a double interface actively interacting with the atmosphere and the ocean (e.g., Delille, 2006; Delille et al., 2014; Heinesch et al., 2009; Rysgaard et al.,

© 2017. The Authors.
This is an open access article under the terms of the Creative Commons Attribution-NonCommercial-NoDerivs License, which permits use and distribution in any medium, provided the original work is properly cited, the use is non-commercial and no modifications or adaptations are made.

2011; Thomas et al., 2010; Zemmelink et al., 2006; Zhou et al., 2013, 2014a, 2014b). It therefore turns out to be much more than a passive pathway between the ocean and the atmosphere for biogeochemical compounds such as greenhouse gases or nutrients. Global climate models however still often consider sea ice as an inert barrier preventing air-sea exchange of gases, limiting therefore gas fluxes to leads and openings within the sea ice cover (Aumont et al., 2015; Steiner et al., 2013; Tison et al., 2002; Vancoppenolle et al., 2013) where wind exchange and turbulent mixing from the sea ice draft are thought to overwhelm the slow diffusion processes within the sea ice itself (Loose et al., 2013; Loose & Schlosser, 2011; Lovely et al., 2015). The few recent attempts to introduce the carbon cycle within sea ice in global 3-D ice-ocean-atmosphere biogeochemical models (Grimm et al., 2016; Moreau et al., 2015, 2016) do not reproduce the very large CO_2 sinks reported in field studies (Else et al., 2011; Heinesch et al., 2009; Miller et al., 2011; Papakyriakou & Miller, 2011; Sievers et al., 2015; Sørensen et al., 2014; Zemmelink et al., 2006) or in simple budget approaches (Delille et al., 2014; Rysgaard et al., 2011).

Sea ice is a multiphase mixture of pure ice, liquid brines, bubbles, and solid salts (often referred to as a "mushy layer", e.g., Notz & Worster, 2009). Its properties are extremely sensitive to those of the ocean and the atmosphere (e.g., temperature, salinity, precipitations, winds. . .). These physicochemical properties in turn control the permeability of the sea ice and therefore internal transport and exchanges with the ocean and the atmosphere.

Among the factors controlling the sea ice physical state, the snow cover has gained particular attention (see Sturm & Massom, 2017 for a review). By insulating the ice cover from the cold atmospheric temperature, it is slowing down ice growth and increasing its internal temperature, therefore increasing permeability for any given salt content. Increased snow depth on the Antarctic sea ice cover is an expected outcome of the predicted intensification of the hydrological cycle in Antarctica, under ongoing global warming (Lenaerts et al., 2016). Increasing snow precipitations in the course of the last century has been recently documented at a coastal continental location east of the Weddell Sea. Philippe et al. (2016) reconstructed 250 years of snow accumulation in a 120 m ice core drilled on the Derwael Ice Rise (70°14'44.88" S, 26°20'5.64" E), coastal Dronning Maud Land, East Antarctica. The mean surface mass balance (SMB, net accumulation) for the whole core amounts to 0.47 ± 0.02 m $_{\text{water equivalent}}$ yr^{-1}. However, the record shows a general increase beginning in the twentieth century, particularly marked during the last 50 years (1962–2011), which yield a mean SMB of 0.61 m $_{\text{water equivalent}}$ yr^{-1}. This paleoclimatic approach of long-term reconstruction of snow accumulation trends is, however, by nature, impossible to follow for the first-year sea ice domain of the Weddell Sea. An atmospheric modeling approach has to be taken instead, following the lines of a recent study by Toyota et al. (2016). These authors searched for the factors responsible of unusually high snow accumulation on pack sea ice off East Antarctica (SIPEX2 cruise, ca. 65°S, 120°E) in late winter 2012. Net snow accumulation rate at the sea ice surface (B) is estimated as follows:

$$\overline{(B)} = \overline{(P)} - \overline{(E)} - \overline{(D)} - \overline{(M)} - \overline{(I)} - \overline{(L)} \quad (1)$$

where P is precipitations rate, E is the net sublimation rate (i.e., sublimation minus deposition and hoarfrost), D is the deposition rate of snow by drifting, M is the divergence of meltwater run-off, I is the conversion to snow ice (ice formed from the freezing of flooded snow at the surface of the sea ice cover), and L is the loss of snow into open water leads and cracks (Leonard & Maksym, 2011). Following the original approach of Bromwich (1988) for the Antarctic continent, these authors consider D and M as negligible compared to P and E, which therefore reduces equation (1) to:

$$\overline{(B)} = \overline{(P)} - \overline{(E)} - \overline{(I)} - \overline{(L)} \quad (2)$$

The net precipitation ($\overline{(P)} - \overline{(E)}$) is then calculated using meteorological reanalysis (6h-ERA-Interim) applying an atmospheric moisture budget equation. This has been done for the 1990–2012 period, both at the regional scale (SIPEX2 cruise domain) and for the whole Antarctic sea ice area. Although this modeling approach could only be validated against the SIPEX2 observations, it gives interesting results. At the scale of the observational area, it shows that no trend is seen in the net annual precipitation over sea ice throughout the 1990–2012 period. This, and the fact that limited snow ice was detected in the SIPEX2 cores ($\overline{(I)}$), led the authors to conclude that the exceptionally high snow depth observed in 2012 resulted from a drastic reduction of the loss of snow to leads and cracks. The authors suggest, based on observed thicker sea ice that year (2012 compared to 2007), that this is the result of a rougher ice surface caused by highly active deformation processes, larger floes, and a wider expansion of the sea ice area in 2012.

As illustrated above, large uncertainties remain on the contribution of sea ice to fluxes of chemical elements between the ocean and the atmosphere. This reflects in a simplistic representation within global Earth System models, stressing the importance of understanding the processes at play from observation data sets. In this regard, a major drawback in previous attempts to pinpoint the annual balance of the impact of sea ice on biogeochemical exchanges with the ocean and the atmosphere is the paucity of autumn and winter data sets. By default, it is often assumed that sea-ice winter biogeochemical activity is restricted by the very low temperatures and light levels (e.g., Delille et al., 2014; Gosselin et al., 1990; Meiners et al., 2012; Vancoppenolle & Tedesco, 2017). Interestingly, however, in their review of historical ice core Chl-*a* data in Antarctic sea ice (8,247 core sections, including 990 profiles), Meiners et al. (2012) report a mean integrated Chl-*a* content of 3.2 mg m^{-2} in June–July–August (versus 6.4 mg m^{-2} annual mean and 12.9 mg m^{-2} for December–January–February), at times where the PAR (Photosynthetically Available Radiation) is negligible (ca. 10 μmol photon $m^{-2}s^{-1}$). This suggests potential residual algal photosynthetic activity during the winter. In this paper, we use the rare opportunity of the AWECS (Antarctic Winter Ecosystem Climate Study) winter cruise in 2013 to show that the default assumption stated above needs to be revisited, especially within the context of a warming world.

2. The AWECS Expedition

2.1. Cruise Context

The AWECS cruise took place between 8 June and 12 August 2013 in the Weddell Sea (Figure 1a, color dots). The main goal of the cruise was to understand how the Antarctic sea ice physical environment affects the seasonal and regional dynamics of biogeochemical cycles, with emphasis on winter processes. One of the more specific topics was to gather a suite of physical and biogeochemical parameters at a series of ice stations, in order to decipher winter sea ice biogeochemical dynamics and the control it exerts on the exchanges across the atmosphere-ice-ocean interfaces. The RV *Polarstern* left Cape Town for a southward transect along the Greenwich meridian, then sailed west toward the Antarctic Peninsula at 68°16 S. The expedition paused for 7 days on 17 July due to medical emergency, then resumed along the Antarctic Peninsula, before heading back North to Punta Arenas (Chile). A total of 11 stations were sampled, for about 12 h each, to provide a full description of the biogeochemical state of the ice cover. Atmospheric conditions alternated between very cold episodes (down to −28°C), with dry southerly wind flow and clear skies, and very warm episodes (up to −0.5°C) corresponding to the passage of oceanic depressions (with high cloud cover and heavy snow fall) travelling eastward across the Weddell Sea, even relatively close to the Antarctic coast (Figure 1c), which has been described previously as typical of the East Antarctic sea ice zone (Worby et al., 1998). This resulted in quite contrasted temperature records between stations (Figure 1b), with drastic changes in the sea ice cover properties, as discussed below.

2.2. Field Activity

At each of the chosen biogeochemical stations (486 to 517 in Figure 1a), a full set of physical and biogeochemical parameters was collected. In this paper, however, we will focus on the basic physicochemical and biological parameters. To support the discussion on the ice cover properties, we will also use the data set from physical transects performed by the ice physics team on board. We briefly expose how these were collected below.

First, the ship was anchored to an ice floe selected in accordance with plans from all the AWECS teams. Care was taken to set up the trace metal clean biogeochemical sampling site upwind of the ship and at a reasonable distance from it (300–500 m). A 10 × 10 m area was then flagged, in which access was only permitted to operators wearing clean suits to prevent contamination (Lannuzel et al., 2006). Power was provided by a 5 kVA generator placed 50 m downwind from the restricted area. A table for ice core treatment, ice core storage boxes, and the various cargo boxes for transport were located in the same area. First, five scientists got dressed with Tyvek clean room garments on top of their polar clothes and plastic bags on their shoes. Snow samples were then taken by one member of the team in the central part of the restricted area. Then, a first core was taken along the lower border of the restricted area. A temperature profile was immediately performed along the core. The core was then stored wrapped in −30°C cooling bags within the core storage box to prevent brine drainage and limit microbial activity. The core was later cut into 0.05 m thick sections for salinity measurements onboard the ship. The drill hole was used to sample water

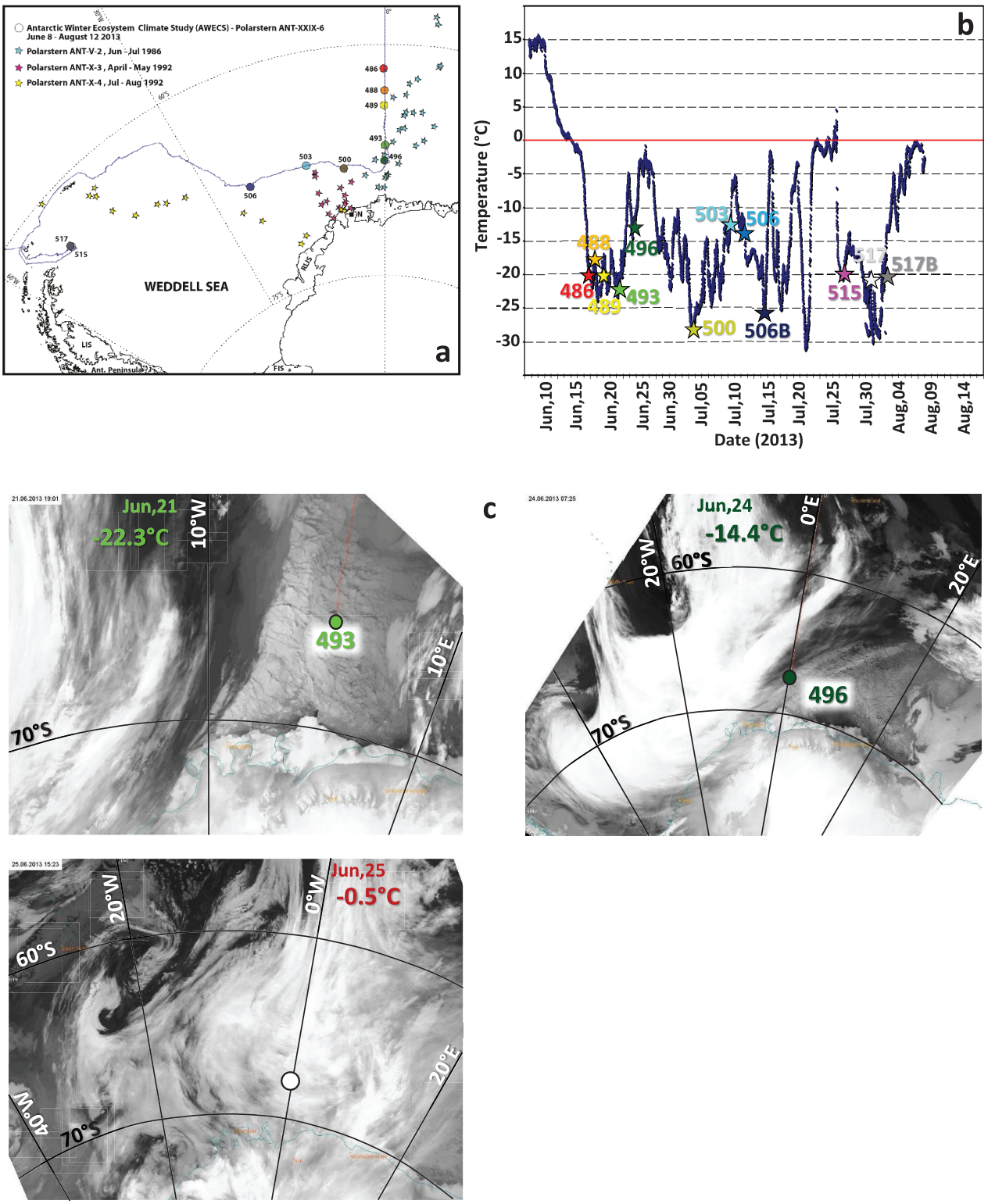

Figure 1. (a) Tracks for the 2013, 1986, and 1992 Polarstern winter voyages, with AWECS 2013 Station numbers; (b) Air temperatures at 29 m height a.s.l. during the AWECS cruise (blue dots) and stations air temperatures at the sampling location (stars); (c) IR satellite maps (credit: NOAA) on 21 June (Station 493), 24 June (Station 496), and 25 June showing contrasted synoptic regimes (red thin line is the Polarstern track, blue thin line is the Antarctic coast).

at various depths. Water was sampled with a noncontaminating peristaltic pump, minimizing the chance of freezing in the sampling tubes.

Meanwhile, "brine sackholes" (incomplete ice core holes reaching a specific depth into sea ice, designed to collect brine, Thomas et al., 2010), were drilled at two different depths. The latter were chosen (based on the temperature profile) so that the shallower one collected brine from the upper impermeable layer (brine volume $<5\%$), and the deeper one from the lower permeable layer. Care was taken not to drill the latter sackholes too deep, to avoid seeping of sea-water upward. For each depth range, six sackholes were drilled in close vicinity to each other to collect enough brines for the various analyses. These were immediately covered with foam corks, to prevent contamination from, e.g., blowing snow or other sources. Note also that, for the same reason, the area was cleaned of its snow cover before drilling. Brine was left to slowly drain into the sackholes typically for a few hours. Sampling was then performed either with the help of a syringe or with a peristaltic pump, when the volumes were sufficient.

Finally, a series of 13 supplementary ice cores were collected in close vicinity to each other (no more than 0.20 m apart). These cores provided material for the whole suite of biogeochemical measurements, and also for some of the experiments to be performed on board. Most drillings were performed using a 0.14 m diameter electropolished stainless steel core barrel.

Sea ice thickness, freeboard (distance between the snow/ice interface and the sea level) and snow depth were measured at eight representative stations (493, 496, 497, 500, 503, 506, 515, and 517, Figure 1a). Discrete manual measurements were performed every 5 m along two crossing transect lines, 100 m long each. Precision of the measurements are within a centimeter for thickness, freeboard, and snow depth.

3. Analytical Methods

3.1. Measurements

Temperature: Ice temperature was measured using a calibrated probe (Testo 720). The probe was inserted into 4 mm holes (matching the diameter of the probe), drilled perpendicular to the ice core axis with a depth resolution of 0.05 m. Precision of the probe was $\pm 0.1^{\circ}$C. Temperature measurements were completed within 5 min after ice core extraction as recommended by Pringle and Ingham (2009).

Bulk salinity: Bulk ice salinity measurements were performed on 0.05 m vertical core sections obtained from the dedicated ice cores. Salinities were measured with a portable electrical conductivity meter (Orion Star Series Meter WP-84TP, calibrated before and after the cruise) on melted ice samples, at room temperature. Vertical cutting for the salinity measurements was performed so that the center of each sample corresponded to the position of the discrete temperature measurements. The precision was ± 0.1.

Thin sections: Continuous ice thin sections ($\sim$600 μm thick) were obtained using a microtome (Leica SM2400), following the standard procedure of Langway (1958). The sections were examined and photographed between crossed polarizers on a universal stage system.

Water stable isotopes: Snow, sea ice, brines, and water δ^{18}O and δD were measured at the Alfred Wegener Institute, following the protocol described in details in Meyer et al. (2000). Briefly, the common equilibration technique was used, with a Finnigan MAT Delta-S mass spectrometer, equipped with two equilibration units. The external errors of long-term standard measurements for hydrogen and oxygen are better than $0.8‰$ and $0.10‰$, respectively.

Chl-*a and Phaeopigments*: For Chl-*a* measurements, a dedicated ice core was cut at a 0.10 m vertical resolution. Samples were melted in the dark, in 0.2 μm filtered seawater (1:4 volume ratio) to avoid osmotic stress. Melted samples were filtered on 10 and 0.8 μm polycarbonate filters in a sequence in order to distinguish larger microalgae species from the smaller ones. Filters were analyzed fluorometrically according to standard protocols (Evans et al., 1987).

Algal cell enumeration, taxa, biomass, and PI curves: These biological measurements were performed on cores different from the ones used for Chl-*a* (although collected within 0.20 m of each other). Two twin sea-ice cores were saw-cut into sections of equivalent depth, the sections pooled together and crushed to obtain a sample large enough to ensure that the various measurements originate from the same sample. The samples were treated following standard procedure described in Rintala et al. (2014), including addition

of a given amount of 0.2 μm filtered sea water in order to avoid organism losses due to cell lysis caused by rapid changes in salinity during melting (Garrison & Buck, 1986; Kottmeier et al., 1987). A dilution factor was then calculated to restore the results at the proper bulk sea ice salinity.

For the live microscopy, 800–1,000 mL of live material was concentrated using a 10 μm net for each section. Concentrated live material was examined with an inverted light microscope (Leica DMIL) equipped with 12.5X oculars and 10X, 20X, and 40X objectives. After the live microscopy, a drop of Lugol was added to the 2.5 mL sample in the microscope cuvette to stop the cell movement and a digital camera (Leica DC300F) was used for documentation of the encountered taxa.

Subsamples were also preserved with acid Lugols' solution in 100 mL brown glass bottles stored in dark at $+4$°C for quantitative algal cell abundance analysis following standard procedure (Ütermöhl, 1958), and examined with the inverted light microscope. Large cells and colonies were counted with 100x magnification over an area that covered one half of the cuvette, and the abundance of single cells and small taxa was counted from 50 random fields with 400X magnification. The cell numbers were converted into carbon biomasses (μg C L^{-1}) using species-specific biovolumes and carbon contents according to Olenina et al. (2006) and Menden-Deuer and Lessard (2000).

Photosynthesis-irradiance (PI) response curves of the sympagic community were measured as ^{14}C-CO_3 incorporation at different light levels following standard procedures (Niemi et al., 1983; Platt et al., 1980; Steemann Nielsen, 1952). Sample volumes of 3 mL with added $NaH^{14}CO_3$ (50 μL, final concentration of 0.33 a μCi mL^{-1}; International Agency for ^{14}C, DHI) were incubated for 2–3 h under irradiance ranging from 0 to 4,000 μE m^{-2} s^{-1}. The activity was measured using a Perkin Elmer Tri-Carb 2900TR liquid scintillation analyzer onboard R.V. Polarstern.

3.2. Data Processing

Several physical variables (i.e., brine salinity, brine volume fraction, Rayleigh number) can be derived from the basic ice temperatures and bulk ice salinity measurements.

Theoretical brine salinity and brine volume fraction: The relative volume of brines in the ice is a crucial parameter since it controls permeability, and therefore the mobility of biogeochemical compounds within the sea ice cover and across the atmosphere-ice-ocean interfaces. It is recognized (Eicken et al., 2004; Freitag, 1999; Golden, 2003; Golden et al., 1998) that, for columnar ice, permeability increases at least 1 order of magnitude above a relative brine volume of 5%, which would correspond to a temperature of -5°C for a bulk ice salinity of 5‰ ("law of fives" in, Golden, 2003; Golden et al., 1998). Brine volumes were calculated here using Cox and Weeks (1983) and Lepparänta and Manninen (1988) relationships, revisited by Petrich and Eicken (2017), neglecting the air volume fraction.

Rayleigh numbers: Rayleigh number (Ra) is used as a proxy for gravity drainage (i.e., brine convection). Ra expresses the ratio between the negative buoyancy in the brines and dissipation (Notz & Worster, 2008). At a given depth z within sea ice, Ra is given by:

$$Ra = \frac{g \cdot (h_i - z) \cdot \rho_w . \beta_w . [\sigma(z) - S_w] \cdot \Pi(e_{\min})}{\kappa \cdot \eta} \quad (3)$$

where g is the gravity acceleration $g = 9.81$ m·s^{-2}, $[\sigma(z)\text{-}S_w]$ is the difference between the brine density at the level z and at the ice-seawater interface, ρ_w is the density of pure water, β_w is the haline expansion coefficient of seawater, with both ρ_w and β_w taken at 0°C from Fofonoff (1985). $\Pi(e_{min})$ is the effective ice permeability (m^2) which is computed using the formula of Freitag (1999) (equation (2.19), p. 48) as a function of the minimum brine volume e_{min} between the level z and the ice-ocean interface. For brine volume fraction, we used the equations given in Notz and Worster (2009). The dynamic viscosity and the thermal diffusivity of brine are $\eta = 2.55\ 10^{-3}$ kg·$(m{\cdot}s)^{-1}$ and $\kappa = 1.2\ 10^{-7}$ m·s^{-2}, respectively, following Notz and Worster (2008).

It is noteworthy that the formulation of Freitag (1999) for ice permeability was developed for young sea ice ($<$0.30 m), and a more appropriate formula would be the one of Eicken et al. (2004) derived from first-year ice at Barrow. However, we chose to compute permeability using the formulation of Freitag (1999) for consistency and comparison with previous work (Notz & Worster, 2008).

3.3. Modeling

In the discussion section, we will compare our sea ice physics observations during AWECS 2013 to those obtained in the few available previous winter cruises in the Weddell Sea (1986, 1992). Along the same lines we will also compare those winter cruises observations to outputs from the NEMO-LIM3 global ocean-sea ice model routinely used in climate studies. The ocean engine of NEMO (Nucleus for European Modelling of the Ocean) is a finite-difference, hydrostatic, free-surface, primitive-equation model (Madec and NEMO-Team, 2016). It is coupled to LIM3 (Louvain-la-Neuve sea Ice Model), a dynamic-thermodynamic sea ice model with a representation of the subgrid-scale distributions of ice thickness, enthalpy, and salinity (Vancoppenolle et al., 2009). The explicit inclusion of brine entrapment and drainage makes the sea ice salinity variable both in space and in time. We use version 3.5 of NEMO, with modifications to the sea ice code that include changes in the time stepping and a reformulation of ice-ocean fluxes allowing to track the different contributions to the ice mass, salt, and heat balances (Rousset et al., 2015).

In the present application, the model was applied to the ORCA1 grid, with a nominal 1° resolution at midlatitudes and increasing toward the poles. The simulation, covering 1948 to 2013, is forced by atmospheric fields combining daily NCEP/NCAR reanalyses of surface air temperature and wind speed (Kalnay et al., 1996) with monthly climatologies of relative humidity (Trenberth et al., 1989), cloud fraction (Berliand & Strokina, 1980), and precipitation (Large & Yeager, 2004). Continental runoff rates are prescribed from the climatological data set of Dai and Trenberth (2002). Such set up has known limitations (Barthélemy et al., 2015), including an underestimation of the summer sea ice extent and the fact that snowfall rates derive from a monthly climatology and therefore do not show any trend during the simulation period. The model outputs that we will consider in this paper are: mean sea ice temperature, mean brine volume (average for

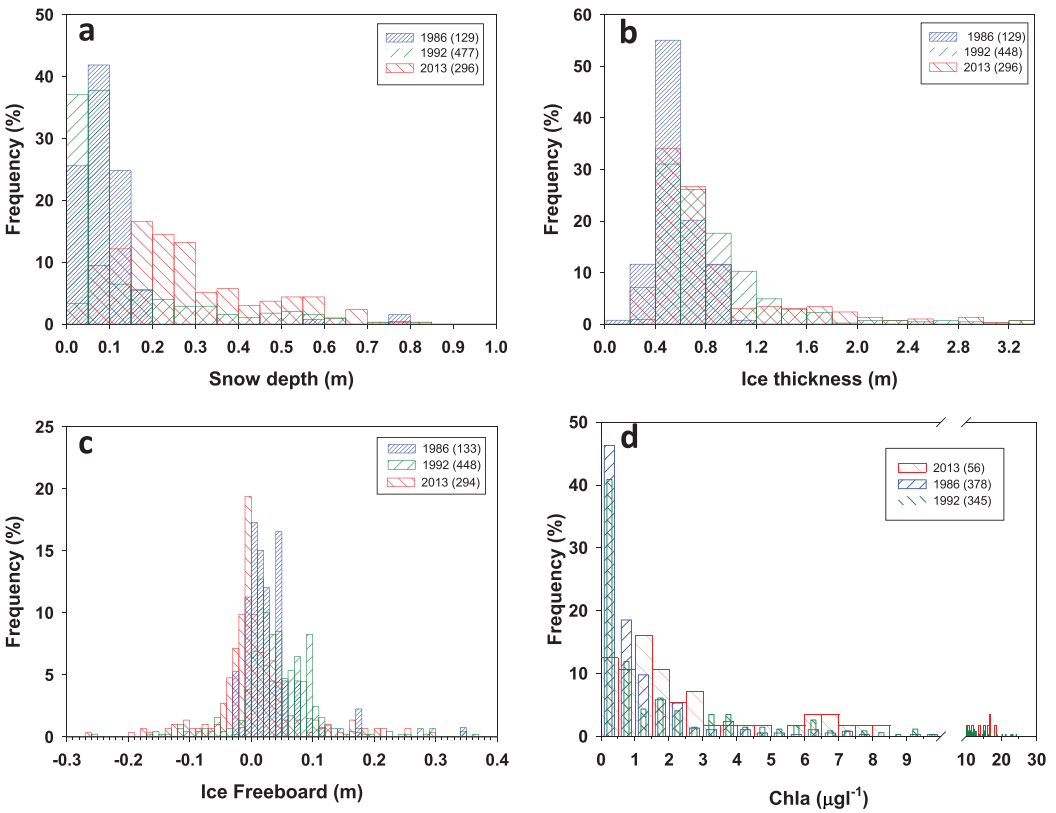

Figure 2. Frequency distribution of observed (a) snow depth, (b) ice thickness, (c) ice freeboard, and (d) Chl-*a* along the (red) AWECS transects, compared to data from previous winter cruises in the Weddell Sea: Polarstern ANT V-2 (June–August 1986, blue) and Polarstern ANT X-4 (July–August 1992, green). Total sample numbers for each group is shown between parentheses. ANT V-2 and ANT X-4 data courtesy of AWI (Alfred Wegener Institute) archive and Prof. H. Eicken.

Table 1
Probability p-*Values From Mann-Whitney Rank Sum Tests for Similarity of Median Values for Snow Depth, Ice Thickness, Ice Freeboard, and Chl-a Concentration for the Three Available Winter Cruises in the Weddell Sea*

		Snow depth (m)	Ice thickness (m)	Ice freeboard (m)	Chl-*a* ($\mu g\ L^{-1}$)
1986–1992	*Medians*	0.08–0.07	0.52–0.71	0.02–0.04	0.56–0.82
	Probability	0.728	***<0.001***	***<0.001***	***<0.001***
1986–2013	*Medians*	0.08–0.23	0.52–0.66	0.02–0.00	0.56–2.04
	Probability	***<0.001***	***<0.001***	***<0.001***	***<0.001***
1992–2013	*Medians*	0.07–0.23	0.71–0.66	0.04–0.00	0.82–2.04
	Probability	***<0.001***	0.006	***<0.001***	***<0.001***

Note. Bold italic values indicate highly significant differences.

five ice thickness categories), and total snow thickness accumulated on sea ice at each pixel over the period of interest.

4. Results

4.1. Snow and Ice Thickness, Ice Freeboard

Figures 2a–2c shows the frequency distribution of observed snow depth, ice thickness, and freeboard along the AWECS (2013, red) transects. It is compared to data from the two previous winter cruises in the Weddell Sea: Polarstern ANT V-2 (June–August 1986, blue) and Polarstern ANT X-4 (July–August 1992, green). ANT V-2 and ANT X-4 data are from AWI archives (courtesy of Hajo Eicken). Probability *p*-values from Mann-Whitney Rank Sum tests for similarity of median values (non-normal distribution) for snow depth, ice thickness, and ice freeboard between the three cruises are given in Table 1. Snow depth distribution shifts toward higher values in 2013 as compared to the previous cruises, with 1992 and 2013 showing a "tail" of larger values. Differences in ice thickness are less clear, apart from a slight (but significant with $p < 0.001$ in terms of median value) increase in 1992 and 2013 as compared to 1986. Positive freeboards clearly dominate the distribution in 1986 and 1992, while it is centered on slightly negative values in 2013. This is a result of the combination of higher snow depth and maybe slightly thinner ice (just not significant in terms of median value with $p = 0.006$) in 2013 than in 1992.

4.2. Ice Texture and Ice Types

Figure 3 summarizes the ice textural properties at each biogeochemical station. As previously reported for the Weddell Sea (Lange, 1990; Lange et al., 1989), frazil ice dominates due to the preponderance of turbulent conditions and of the pancake cycle in the region. This is also seen in the signs of rafting (alternation of frazil and columnar layers) visible in some of the cores (489, 500, 506b). Another interesting feature is the regular occurrence of linear vertical brine tubes, generally in the upper 0.30 m of the cores (e.g., AW500 left in Figure 3, but also reported at stations 493, 496, and 506b). Along the Antarctic Peninsula the facies differ, with locations of calmer thermodynamic growth of columnar ice (stations 517 and 517b), or influence of coastal processes (thicker ice and platelet ice formation-e.g., 0.25-0.40 m and 1.05-1.15 m-station 515). Texture and thickness at all stations (to the exception of Station 515) suggests we are dealing with first-year pack ice. Note that station 515 is indeed a special case. Its higher thickness (>1.75 m) makes it a potential candidate for young second-year ice. Occurrence of platelet ice suggests proximity of an ice shelf along the coast, and large accumulation of compacted frazil of low salinity (see below, Figure 4d) could point to the marginal ice zone of a polynya. This first-year landfast sea ice would then have detached and been entrapped in the newly forming winter ice, promoting it to young second-year ice (having survived one summer).

4.3. Ice Temperature

Figure 4a summarizes 2 m air (squares), snow surface (upward pointing triangles), snow-ice interface (downward pointing triangles), and ice (positive depths) temperatures. Complementarily, the figure also shows local snow depth at the biogeochemistry station (mean of 10 values) and, for the strongly flooded station 500, the limit between dry and wet snow (triangle with cross) and the water level in

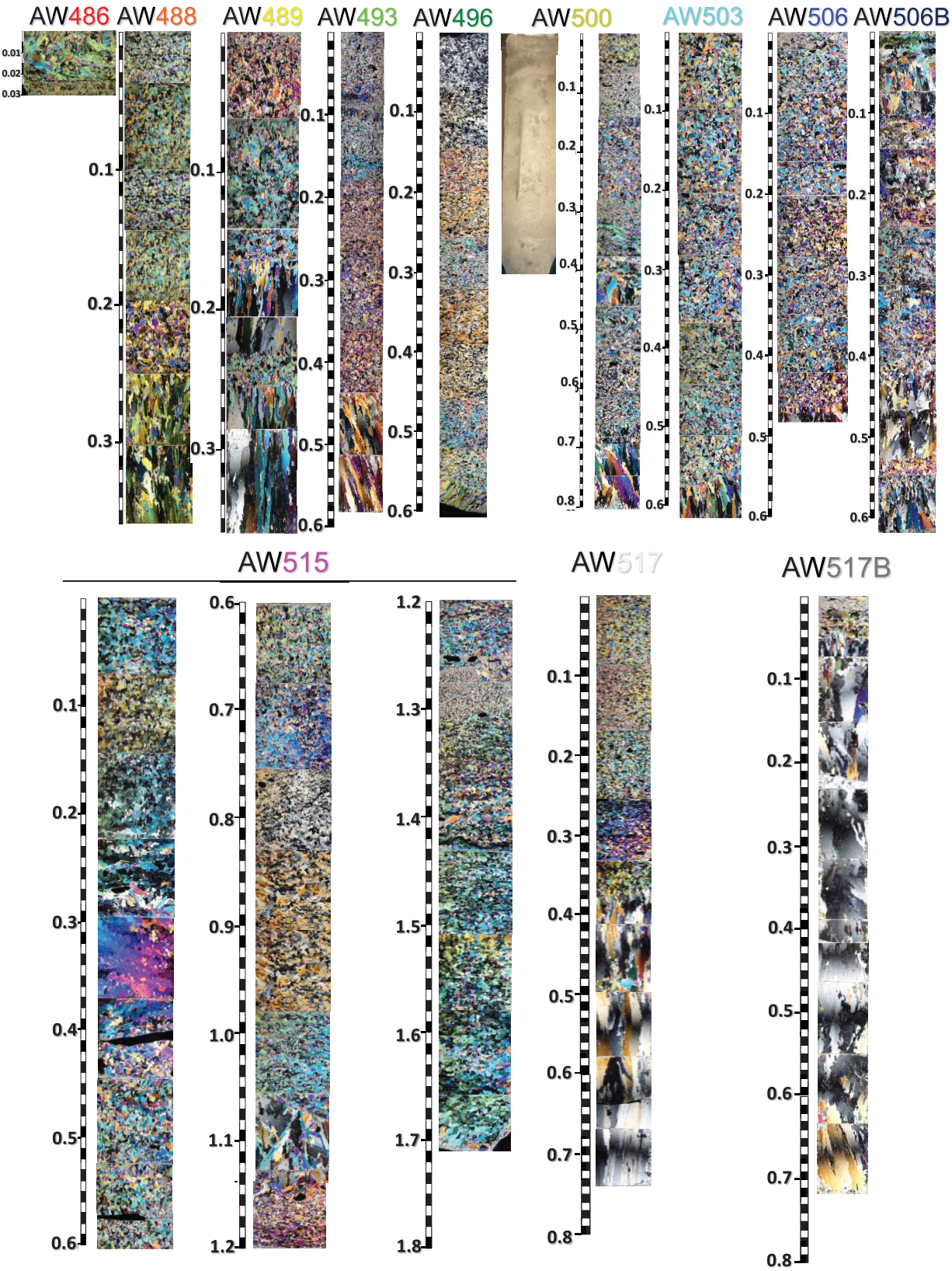

Figure 3. Textural characteristics of the AWECS ice cores. See Figure 1a for Stations location. Depth scale in meters.

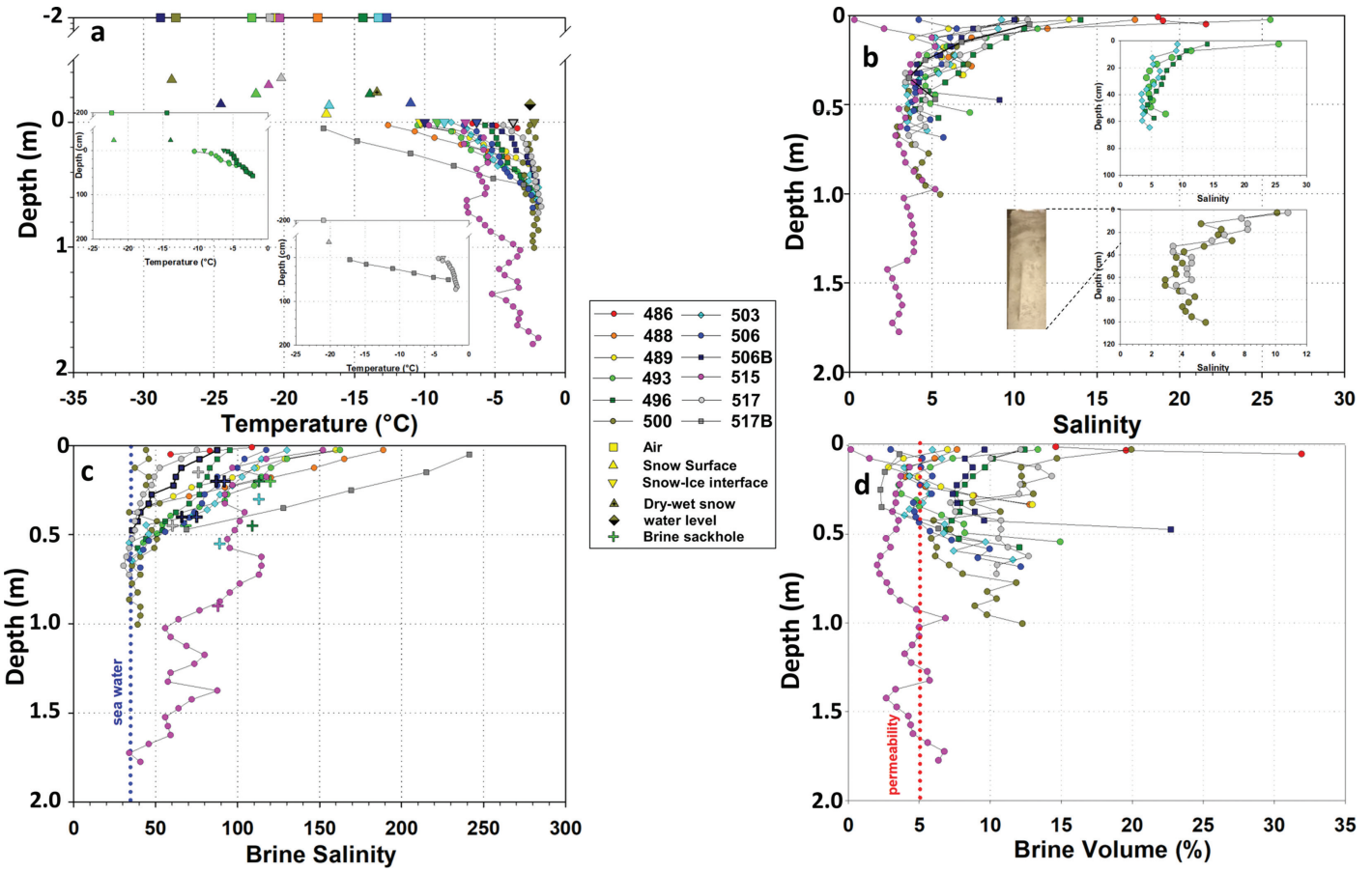

Figure 4. Basic and derived physicochemical properties of the AWECS ice cores: (a) air-snow-ice temperature, (b) bulk ice salinity, (c) brine salinity, (d) brine volume. Blue dotted line in Figure 4c is sea water salinity. Red dotted line in Figure 4d is the 5% permeability threshold from Golden et al. (1998). Left insert in Figure 4a isolates profiles 493 and 496 (temperature effect); Right insert in Figure 4a isolates profiles 517 and 517b (snow thickness effect). Top insert in Figure 4b isolates profiles 493, 496, and 503, Bottom insert in Figure 4b isolates profiles 500 and 517 (local salinity maximum). See text for details.

the snow (two colors diamond). Large temperature differences are seen between air, snow, and ice. Because of the generally deep snow cover (see section 4.1), the ice is globally quite warm for the middle winter period (mean value of −4.5°C for all samples). This is clearly illustrated by the individual comparison of stations 517 (0.354 m snow cover) and 517b (same day and same location, no snow cover) in the lower insert of Figure 4a. An important controlling factor of ice temperatures is the large range of air temperatures encountered during the study, even at a few days interval, as shown by the comparison of stations 493 and 496 with similar snow depth (upper insert in Figure 4a). Another important consequence of the thick snow cover is the frequent occurrence of flooding events, sometimes bringing the snow-ice interface temperature (downward pointing triangles) very close to sea water freezing point (e.g., Station 500).

4.4. Ice and Brine Salinity

Bulk ice salinity profiles (Figure 4b) show a classical C-shaped profile in most cases. Particular features are: (a) the very high salinity of the pancake ice Station 486 sampled in the marginal ice zone, (b) the surface salinity decrease at stations 506 and 515, (c) a relative maximum between 0.10 and 0.40 m depth at stations 493, 496, 503 (upper insert in Figure 4b), 500, and 517 (lower insert in Figure 4b) the generally low salinity and jagged profile at station 515.

Brine salinity profile (Figure 4c) is the mirror image of the temperature profile because of the phase equilibrium assumption made in the calculations, with most values above sea water salinity, apart from the bottom sections. Brine salinity measured in the sackholes (crosses, usually two depths at each station) is systematically higher than the calculated values at depth, probably due to the percolation of brine from the surface layers.

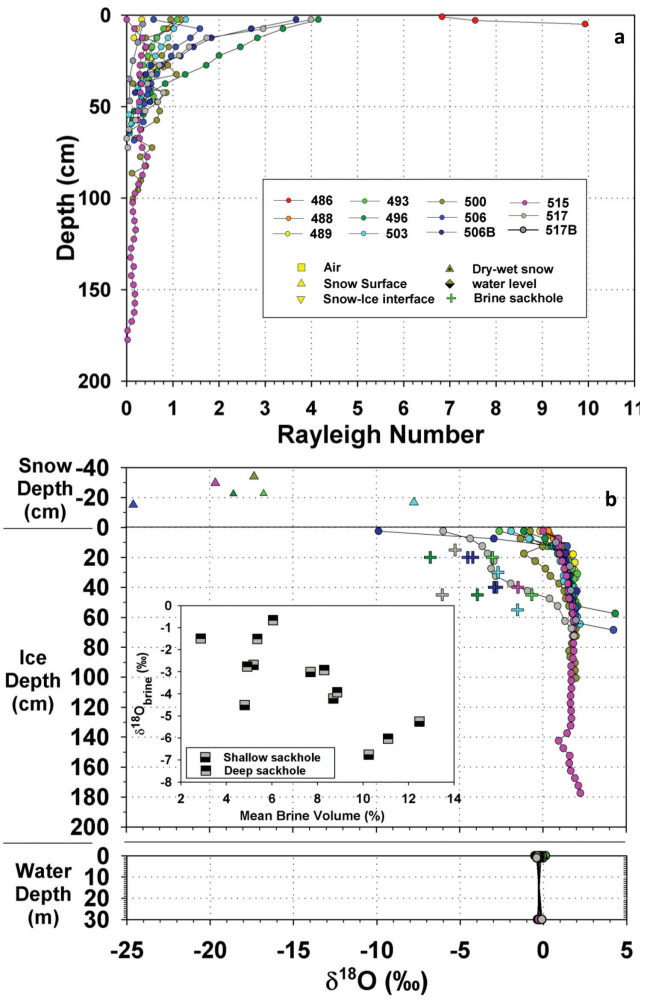

Figure 5. (a) Rayleigh numbers and (b) $\delta^{18}O$ (b) profiles for the AWECS biogeochemical stations. Stations color caption as in Figure 4. Insert in Figure 5b shows the $\delta^{18}O_{brine}$ versus mean brine volume relationship. See text for details.

4.5. Brine Volumes and Rayleigh Numbers

Because the ice temperatures remained rather warm at AWECS, a high number of stations show a brine volume above the permeability threshold (red-dotted line in Figure 4d). Impermeable ice, was limited to some internal layers and to a few surface layers with low bulk ice salinity. An obvious exception to this pattern is the profile at the thicker ice station 515, where brine volumes are generally below or slightly above the permeability threshold.

Rayleigh numbers (Figure 5a) further document potential brine motion in permeable ice. Denser (colder and more saline) brines will initiate convective movement in permeable ice where the destabilizing density gradient overcomes stabilizing forces (see equation (1)). The value of a threshold Rayleigh number is however today still a matter of debate (Carnat et al., 2013; Hunke et al., 2011; Notz & Worster, 2009), depending on many assumptions in the calculations, hence the interpretation can only be qualitative today. In Figure 5a, we surmise that active convection only existed for a few stations at the time of sampling: 486, 496, 506b, and 517.

4.6. Water Stable Isotopes: δD and $\delta^{18}O$

Figure 5b shows the $\delta^{18}O$ profiles in snow, ice, and waters at the AWECS stations. Co-isotopic diagrams (δD versus $\delta^{18}O$) are plotted in Figure 6, also for different subgroups of samples, with associated regression lines and equations. Sea water is very close to SMOW (Standard Mean Ocean Water) with mean values in $\delta^{18}O$ and δD of respectively -0.27 and -2.83 ‰. In the co-isotopic diagram (Figure 6), snow samples near-perfectly ($r^2 = 0.999$) align on a regression line with a slope of 7.98, as expected for a Meteoric Water Line. Sea ice samples define a very good ($r^2 = 0.89$), regression line with slope of 6.81 (Figure 6c). Brine samples very well align ($r^2 = 0.99$) on a slope of 7.70, with an equation of the regression line remaining unchanged when sea water samples are added to the group (Figure 6b). They all show more negative values (between -0.5 and -8 ‰) than the bulk ice from which they were collected (crosses in Figure 5b), and show a global relationship of decreasing $\delta^{18}O$ with increasing brine volume (insert in Figure 5b).

4.7. Chlorophyll-a and Phaeopigments

Figure 7 summarizes the results of Chl-*a* and Phaeopigments analyses performed during the study, together with a few ancillary measurements: snow depth, freeboard (where available), and the detection of "brine tubes" (BT, see e.g., core AW500 in Figure 3) in the treated cores. Mean (SW) values are also given for three discrete sampling depths in the underice water column (interface, 1 m and 30 m). For ice Chl-*a*, a distinction is made between small (from 0.8 to 10 μm, in light green) and large (>10 μm, dark green) autotrophs. Globally, an internal algal community dominates along the Greenwich meridian and in the central Weddell Sea (station 496 also has a bottom community), while a bottom community dominates along the Antarctic Peninsula, where the Chl-*a* levels are also lower in the first year ice. The majority of the Chl-*a* corresponds to the larger organisms, and there is a general trend of increasing Chl-*a* levels from the marginal ice zone toward the Antarctic coast. Generally, also, brine tubes are observed at the stations with the highest Chl-*a* levels.

Figure 7 also shows the Phaeopigments/Chl-*a* (P/Chl-*a*) ratio profiles in ice for all stations. As discussed in section 5.2, this ratio can be interpreted in terms of algal community health and active growth. Several features emerge. Sea water Chl-*a* values (0.01–0.11 μg L^{-1}) are always negligible compared to ice concentrations, with, however, slightly higher values in the northern stations. P/Chl-*a* in sea water generally increase southward, from 33% to 334%. Ice Chl-*a* and P/Chl-*a* values are low in the marginal ice zone station 486,

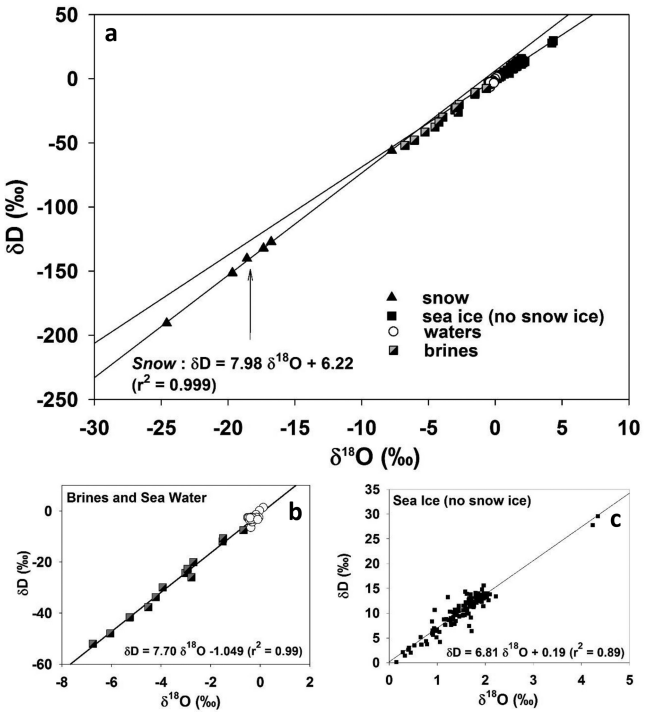

Figure 6. Co-isotopic signatures of snow, sea ice, brines, and waters at AWECS: (a) all samples; (b) brines and sea water samples; (c) sea ice samples (excluding snow ice samples).

and similar to sea water values. In the eastern Weddell Sea (stations 488 to 506b), P/Chl-*a* ratios remain low (between 2 and 30%) compared to sea water values (33 to 260%). Along the Antarctic Peninsula, the ice P/Chl-*a* ratios increase to maximum values of 50–60%. The P/Chl-*a* ratios also show a general inverse relationship to total Chl-*a*, with lower values in layers of higher Chl-*a* concentrations. These include the bottom layers of stations 496, 517, and 517b, all showing a local Chl-*a* maximum.

4.8. Biological Characteristics at Stations 506-506b

Because of the very strong contrast in Chl-*a* concentrations between stations 506 and 506B (less than 20 m apart and sampled at 4 days interval—Figure 7), it has been chosen to document the structure of the algal communities in more details at those stations. Figures 8c, 8d and 8e, 8f describe the algal speciation at locations 506 and 506b, respectively, in terms of number of cells (c-d) and in terms of biomass (e-f, μgC L^{-1}ice). Figure 8g presents the Photosynthesis-Irradiance (PI) curves of five successive and continuous layers spreading the whole ice thickness of Station 506b.

The number of cells is higher by nearly an order of magnitude at 506b compared to 506 and the biomass by roughly a factor two. While diatoms and dinoflagellates dominate the sympagic population at 506, 506b is overwhelmed by small ($<$10 μm) unidentified flagellates, with total absence of dinoflagellates. Note, however, that diatoms are still in larger number at 506b than at 506. In terms of biomass, while dinoflagellates dominate the community at 506, diatoms take over at 506b, increasing their biomass in a given layer from about 75 μgC L^{-1}C to up to 400 μgC L^{-1}C. Because of their small size, unidentified flagellates cannot compete with diatoms in terms of biomass, and remain a small fraction of the total biomass.

Figure 8g shows the PI curves for 5 successive and continuous layers of Station 506b. The main features are: (a) the rapid photosynthetic response at low irradiance (the steep slope of the start of the PI curve indicates high photosynthetic efficiency at low irradiances—in the 10–100 μmol photons $m^{-2}s^{-1}$ range) and (b) the decrease of the photosynthetic rate above a few hundreds μmol photons $m^{-2}s^{-1}$, suggesting photoinhibition in the lower layers (bottom 0.25 m) of the sea ice cover.

5. Discussion

5.1. A Dynamic Winter Sea Ice Brine System

Our knowledge of winter Antarctic sea ice remains extremely limited. It has often been assumed that the sea ice brine system would evolve toward a closed system in this very cold and dark environment, with limited biogeochemical activity and exchanges. Results from this study are challenging that perspective. As documented in Figures 1b and 1c, regular intrusions of large-scale synoptic depressions well into the Weddell Sea resulted in a very dynamic air temperature record, with weekly excursions between -30°C and near-zero temperatures (with even slightly positive values near the Antarctic Peninsula). This in turn contributed to large excursions in the internal sea ice temperature, however with a slight delay and often limited in amplitude due to the insulating role of the snow cover. Snow also favored flooding of the ice cover surface, and subsequent warming, by depressing the snow-ice interface below sea level. The frequency distribution of freeboard records (Figure 2c, red bars) indeed shows a slightly negative median value. This had two main consequences: (a) the frequent occurrence of a surface snow ice layer about 0.10 m thick (with maximum of 0.30 to 0.45 m at stations 500 and 517—detected by negative δO^{18} values in the profiles of Figures 5b and 5b) snow-ice interface temperatures episodically reaching values close to the sea water freezing point (see station 500 in Figure 4a, with a quasi-isothermal ice temperature profile).

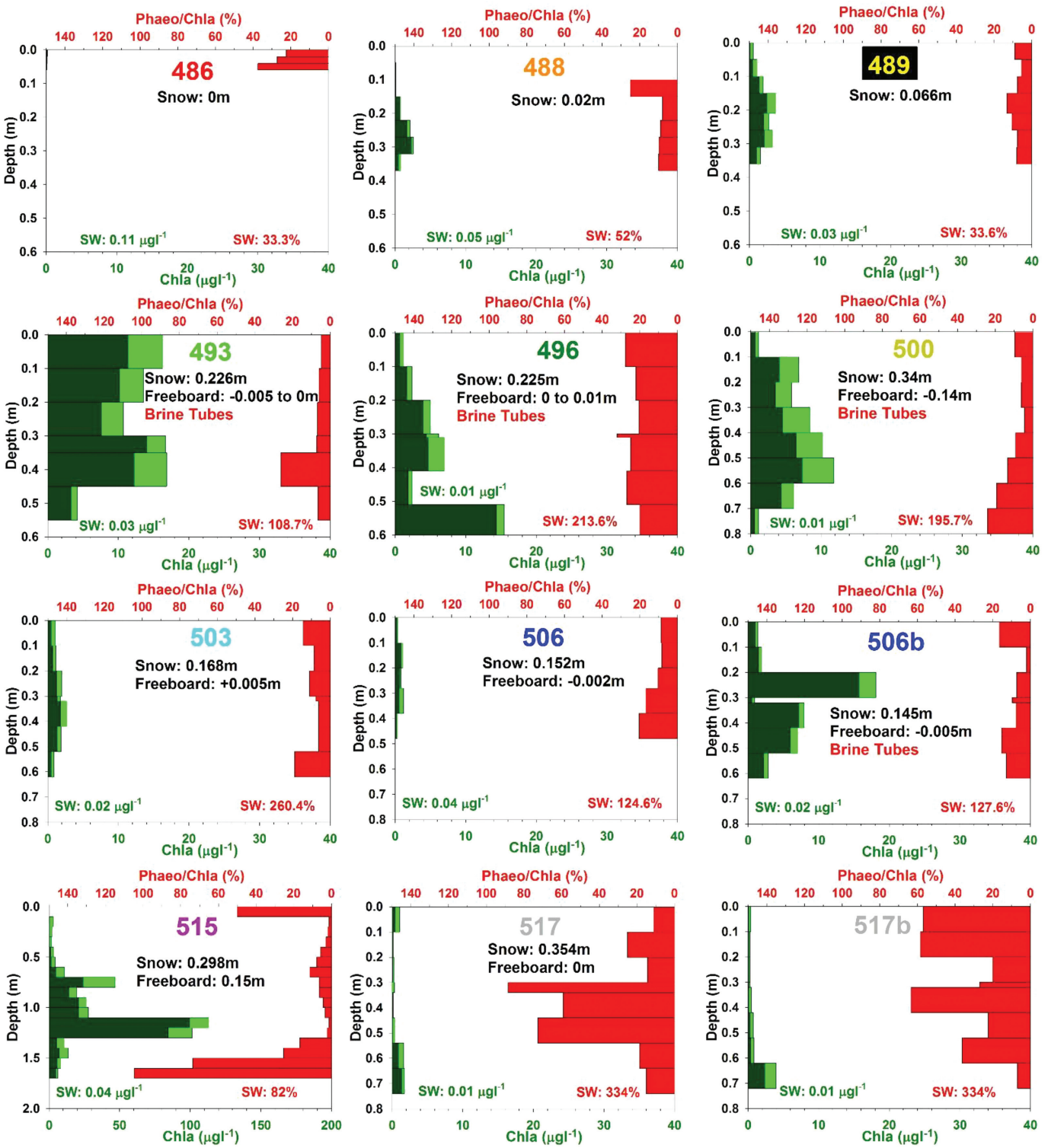

Figure 7. Chl-*a* concentration in μg L_{ice}^{-1} (> 10 μm size in dark green; between 0.8 and 10 μm size in light green) and Phaeopigments/Chl-*a* ratio profiles in % (red) at the AWECS stations. SW = mean sea water values for three discrete sampling depths: ice-water interface, 1 and 30 m. Also indicated for reference, where measured: Snow thickness in meters, Freeboard in meters, and occurrence of brine tubes in the sampled cores.

Although only station 506 was revisited after a few days (506b), the comparison of their temperature profile (Figure 4a), with similar snow depth (0.152 versus 0.144 m), clearly shows large ice temperature excursions within a few days. Similar temperature swings may hold at larger scales in the Weddell Sea in the course of

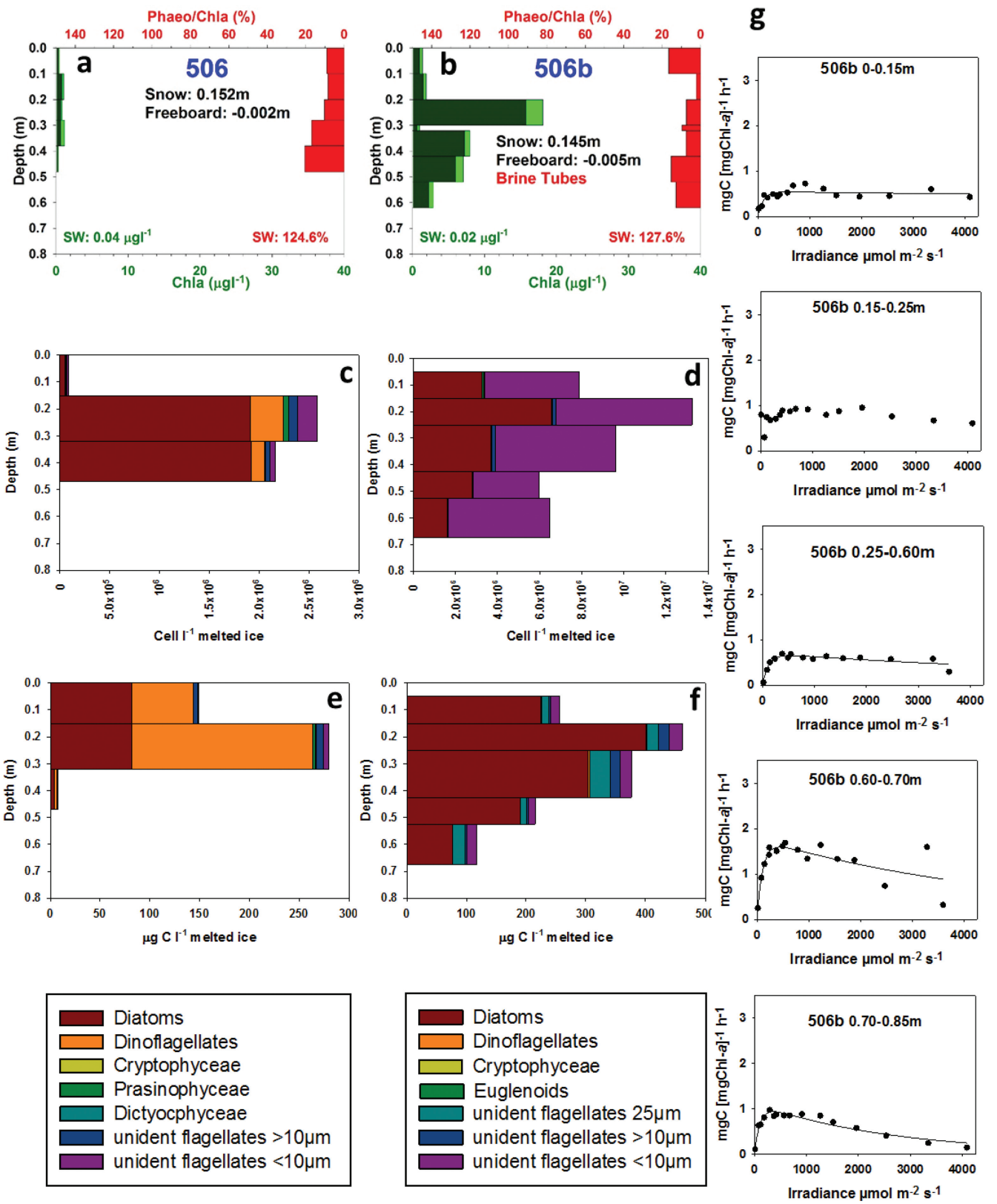

Figure 8. Biological characteristics at Station 506 (a and b are 4 days and 20 m apart)—(a and b) Chl-*a* (dark green = >10 μm; light green = 0.8–10 μm) and Phaeopigments to Chl-*a* ratio (%, red); (c and d) number of cells per liter of melted ice; (e and f) biomass in micrograms Carbon per liter of melted ice; (g) PI curves for five successive and continuous layers of station 506b. Note the difference in scales between 8c–8d and 8e–8f. See text for details.

the winter, due to the repeated shifts of relatively cold continental air and warm oceanic depressions. The process is in fact similar to what has been observed during the SIMBA spring cruise (NBP0704, Bellingshausen Sea, October 2007, Carnat et al., 2016; Lewis et al., 2011).

A direct consequence of these temperature contrasts is the unusual occurrence of elevated Rayleigh numbers in the upper half of the ice cover at some stations (Figure 5a). Indeed, elevated Rayleigh numbers are usually encountered within the bottom layers of thermodynamically growing sea ice (Carnat et al., 2013; Notz & Worster, 2009; Zhou et al., 2014b), which is actually the case in none of the AWECS stations. High Rayleigh numbers in the upper sea ice cover are rather typical of warming spring sea ice, leading to episodic brine convective events across the whole ice cover (e.g., Zhou et al., 2013). At the SIMBA spring stations, "brine tubes," initiating close to the ice cover surface, and sometimes extending all the way to the bottom were reported (e.g., Lewis et al., 2011, Figures 8 and 11). Brine tubes morphology differs from that of brine channels. While the latter usually show a funnel-like geometry, with adventitious secondary channels converging toward a central main drainage channel, brine tubes are generally broader linear single features. Brine tubes were observed in several of the AWECS stations (493, 496, 500, 506b—Figures 3 and 7), but generally limited to the upper 0.30-0.40 m of the ice cover. We suggest that they result (as it was the case at the SIMBA process stations) from the combination of flooding and temperature cycling in the ice. During the cooling phases, surface sea water and brines partly refreeze which increases brine salinity. During the warming phases, these high salinity brines thermodynamically readjust, progressively dissolving the snow/ice as they move downward under gravity, forming the brine tubes. The latter materialize salts transport downward, a movement which is sometimes witnessed by a local maximum in salinity at those depth (see inserts of Figure 4b). At the SIMBA Spring stations, the process was intense enough for brine tubes to reach all the way to the bottom of the sea ice cover, with visible plumes of denser brine protruding below the ice-water interface (Lewis et al., 2011, Figure 11). This process, which can repeat itself several time in the history of the sea ice cover at a given location, together with the globally high brine volumes generated by the warm ice temperatures (Figure 4d) supporting permeability, would turn the sea ice cover into a potentially very dynamic biogeochemical environment, brine transport supporting nutrients, gases, and sympagic organisms' movements as well (see section 5.2).

Stable isotopes data also help in better understanding the dynamic of the winter sea ice brine system during AWECS. Snow samples span a large range of negative values (–8 to $-25\ ‰$), reflecting different temperatures of formation or cloud history during the precipitation phase of the hydrological cycle. Sea ice samples, resulting from the freezing of sea water with $\delta^{18}O$ values very close to $0‰$ (–0.27‰), are enriched in heavy isotopes and show steadily increasing $\delta^{18}O$ values with depth (Figure 5b), under the combined effect of snow ice contribution in the surface layers (Jeffries et al., 1994, 1997; Lange et al., 1990) and of a decreasing freezing rate downward (Eicken, 1998; Souchez et al., 1988). Snow ice, as mentioned before, shows negative values, due to the contribution of snow in various proportions. Brines $\delta^{18}O$ are always more negative than the bulk ice values in the equivalent ice profile. This can only be explained in two ways: (a) either it is the remnant signature of the interstitial water of the skeletal layer, later entrapped in the ice, that gets impoverished in heavy isotopes while the solid ice gets enriched during growth at the dendritic interface, or (b) it is the signature of infiltrated melted snow. The inverse relationship ($r^2 = 0.69$) between $\delta^{18}O_{brine}$ and the mean brine volume shown in the insert of Figure 5b supports the latter option. Indeed, increasing brine volume during ice warming from internal ice melting only (with positive δ values), would increase the $\delta^{18}O_{brine}$. Co-isotopic stable isotopes values shown in Figure 6 further support option (b). In this diagram, snow samples closely align on a meteoric line of slope close to 8 (7.98). Note that the local sea water plots slightly below that line, probably due to local contribution of sea ice melt from previous summer. Sea ice samples align on a lower slope of 6.81 (Figure 6c), not very far from the expected freezing slope of 6.98, calculated from the observed sea water values (Jouzel & Souchez, 1982; Souchez et al., 1987; Souchez & Jouzel, 1984). If the brine samples were mainly reflecting the signature of the remnant of interstitial water entrapped during closed system ice growth, they should lie on the same freezing slope. This is not the case since those brine samples are extremely well aligned ($r^2 = 0.99$) on a different slope of 7.70 (Figure 6b). Water samples also lie on that slope, which cross-cuts the meteoric water line at a value of $\delta^{18}0 = -25‰$, suggesting that this best fit line reflects a mixing line between sea water and melted winter snow, replacing the original freeze-on signature due to the history of brine movement within the sea ice cover. This also suggests that snow melting actively contributes to the thermodynamic adjustment of surface brines during warming events.

5.2. A Significant Sympagic Algal Community: Active or Inherited?

The sea ice winter Chl-*a* concentrations reached more than 15 μg L^{-1} in several occasions at the AWECS stations (Figure 7), while the "all-stations" mean value for 0–30 m ocean water was 0.01 μg L^{-1} (n = 27; range: 0.00–0.11 μg L^{-1}). With an average Chl-*a* inventory of 2.44 mg m^{-2} (excluding the Peninsula), the AWECS stations remain close to the average June–July–August value of 3.2 mg m^{-2} obtained in the ASPeCt data review of Meiners et al. (2012), compiling 425 measurements for that season, across the 1983–2008 time period. However, the AWECS data set shows a significantly higher median Chl-*a* concentration than the similar winter cruises of 1986 and 1992 (Figure 2d and Table 1), with a somewhat higher frequency of Chl-*a* maxima (Figure 2d).

Concentrations globally increased along the Greenwich meridian toward the Antarctic coast, with a strong contrast both in total concentration and vertical distribution between the Central Weddell Sea and the Antarctic Peninsula (stations 515, 517, 517b). Ice texture (Figure 3) seems to have played a determining role in this case. Central Weddell Sea samples (486–506b) are predominantly made of granular ice as a result of the well-known pancake cycle in the area (Lange, 1988, 1990). The traditional view is that scavenging processes associated to frazil accumulation in pancake ice is efficient in enriching the internal layers with living material (Garrison et al., 1983; Gradinger & Ikävalko, 1998). On the opposite, columnar ice growth tends to keep the algal community within the bottom layers, as observed for the stations along the Antarctic Peninsula (e.g., 517, 517b), and results in lower Chl-*a* concentrations during the winter. Even in the central Weddell Sea, it appears that intermittent layers of columnar ice are less rich in Chl-*a* (see e.g., 489 around 0.20 m depth; 493 bottom, 506b bottom). Record Chl-*a* concentrations are observed at the young second-year ice Station 515, the highest of which (>100 μg L^{-1}) being located in the platelet ice layer, known as the most productive environment in Antarctic sea ice (Arrigo et al., 1995; Smetacek et al., 1992).

A crucial interrogation is to know if these sympagic communities are passive witnesses of past growth during the early autumnal days of sea ice build-up, or if they are still actively growing at the time of observation. Increasing Chl-*a* concentrations southward along the Greenwich meridian (486–493), suggests that older ice would allow longer time for autumnal sympagic communities to grow, although this does not rule out that these were still active at the time of sampling. On the other hand, the presence of a Chl-*a* maximum in the recently growing bottom columnar ice at station 517/517b, suggests that the algal population there is contemporaneous and therefore still actively growing. Traditionally, it is considered that given the very low light levels in the winter, autotrophy should be negligible (Gosselin et al., 1990; Meiners et al., 2012; Vancoppenolle & Tedesco, 2017). A striking contrast in Chl-*a* concentration profiles was observed between stations 506 and 506b that were sampled at the same location (10–20 m apart) at 4 days interval. Station 506b was sampled the last, at a time when the ice was still warm (Figure 4a) and showing high brine volumes (Figure 4d), while the air temperature was switching again toward very low temperatures, a favorable period for surface brine migration downward in brine tubes. Because of these contrasted properties, these two stations were chosen to document further their biological properties and try to identify potential algal winter growth (Figure 8).

A first simple question would be to know if the observed very large increase in Chl-*a* concentrations could have resulted from active growth during the 4 days interval, or if it is simply the expression of spatial variability of algal outcrops within sea ice (Arrigo et al., 1997; Eicken et al., 1991; Mundy et al., 2005). A very simple calculation would consist in applying a maximum growth potential of 1.5 divisions per day (Guillard, 1973; Wood et al., 2005) during 4 days to the initial (506) population of diatoms of 1.92 10^6 cells L^{-1} (Figure 8c). The result of 11.54 10^6 cells L^{-1} is above the number of diatom cells actually observed at 506b (6.57 10^6 cells L^{-1}, Figure 8d), making the hypothesis plausible. However, the main feature of the comparison between cell numbers at 506 and 506b is the distinct increase in the number of <10 μm unidentified flagellates, that can in no way be solely explained by similar maximal growth rates (maximum of 0.33 10^6 cells L^{-1}. versus observed of 6.45 10^6 cells L^{-1}). It is worth noting that comparing the two stations in terms of species biomass (in micrograms carbon per liter of melted ice, Figures 8e and 8f) the contribution of <10 μm unidentified flagellates remains moderate in 506b due to their low specific biomass (per unit cell). On the contrary, the biomass of the larger diatom cells is higher in 506b by nearly an order of magnitude, corroborating the dominance of larger cells in the Chl-*a* signal (Figure 8b, dark green).

Further clues to active growth can be retrieved from the Photosynthesis-Irradiance (PI) curves shown for Station 506b in Figure 8g. First, the fact that the sympagic algae are indeed responding to light is a clear

sign that their photosynthetic apparatus is in good conditions. Second, the slope of the photosynthetic response at low irradiances (photosynthetic efficiency) is steep, with responses at irradiances in the 10–100 μmol photon m^{-2} s^{-1} range. Gosselin et al. (1990, Figure 2) measured similar irradiances (10–30 μmol photon m^{-2} s^{-1}) in the Canadian Arctic, below 0.15-0.40 m of snow. This snow depth range is similar to the one observed in the present study. Last, the occurrence of photoinhibition above a few hundreds of μmol photon m^{-2} s^{-1} in the lowest 0.25 m of Station 506b (and not above) indicates adaptation to very low light levels.

Low values of phaeopigments to Chl-*a* (P/Chl-*a*) ratios have been interpreted in the past as proof of little degradation of the Chl-*a* pool and also indicators of favorable growth conditions (e.g., Arrigo et al., 2014; Mock et al., 1997). In the Arctic, Zhou et al. (2014b) provide a time series of P/Chl-*a* profiles in ice at Barrow from 3 February to 5 June. Spring ice P/Chl-*a* values are around 20%, with Chl-*a* levels ranging between 0.5 and 80 μg L^{-1}. In early summer, these values reached 40–70% where Chl-*a* was present in significant amounts, and up to 100% elsewhere. At the same location, Krembs et al. (2011, Table S2) reported values of about 222% in the ice and only 22% in the water at the interface, for degrading summer ice (June 2001). Elsewhere in the Arctic (Barents and Greenland seas), Mock and Gradinger (1999) measured P/Chl-*a* values ranging from 3 to 71% in May–June 2007, with minimum values (1%) in the bottom first cm, richest in Chl-*a* (5–80 μg L^{-1}). These authors also show, at several stations, a trend of decreasing P/Chl-*a* (50 to less than 10%) with increasing Chl-*a* (1–80 μg L^{-1}) in the bottom 0.10 m. In the Baltic Sea, Mock et al. (1997) also measured P/Chl-*a* ratios usually ranging between 0 and 20% in February sea ice at Kiel Bight, with Chl-*a* between a few and 20 μg L^{-1}. Finally, for a recent summer Antarctic cruise (December–January 2014) in the Amundsen-Ross seas, Arrigo et al. (2014) report P/Chl-*a* values of 2.4, 3.9, and 5.5% for, respectively, high light interior, low light interior, and bottom environments, out of 17 cores. From all these measurements, it appears that Spring/early Summer sea ice, with active primary production, is characterized by low P/Chl-*a* ratios, while the latter tend to increase as the ice ages and decays.

Most of our AWECS sea ice samples show low P/Chl-*a* values (0–30%), including the bottom communities with a local Chl-*a* maximum (suggesting active growth) at stations 496, 517, 517b. There is also a general trend of decreasing P/Chl-*a* values at higher total Chl-*a* contents. This is in strong contrast with the values of this ratio in surface waters, showing a dominance of phaeopigments as one progresses southward within the pack (33%–334%). This clearly supports the potential for actively growing algae within the interior layers of our winter sea ice at AWECS.

In summary, although it is not precluded that the strong contrast between stations 506 and 506b could result from initial environmental patchiness at the time of ice growth (autumn), several indicators suggest that active algal growth at the period of sampling is also involved, and that this might also be true for the other AWECS stations. Regular invasion of the internal community due to flooding and increased permeability might have played a crucial role in this active growth. The latter would be corroborated by the large increase in brine volume between 506 and 506b, the presence of brine tubes, the strong increase of the very small ($<$10 μm) unidentified flagellates, the photosynthetic efficiency at low irradiances, the adaptation to very low light levels and the observed very low P/Chl-*a* ratios in the ice, in strong contrast with the sea water values. Note that water Chl-*a* concentrations are at 0.01 μg L^{-1} for both stations, ruling out simple passive entrainment in the ice during flooding, to explain the observed Chl-*a* levels. Clearly, future work should involve "in-situ" incubation experiments (e.g., Mock, 2002; Mock & Gradinger, 1999; Smith & Herman, 1991; Song et al., 2016) to further document this potentially active photosynthetic activity in the middle of the winter.

5.3. A Changing Antarctic Sea Ice in the Weddell Sea?

Data on winter Antarctic sea ice properties are scarce, and, for the Weddell Sea, only three winter cruises are available, including the AWECS cruise described in this paper. As pointed out in the description of Figure 2 in the results section, interesting contrasts however seem to emerge. The 2013 snow depth distribution is clearly shifted toward higher thickness classes as compared to 1986, a situation that seems to initiate in 1992 already (Figure 2 left, Table 1). While the ice thickness median is significantly higher in 1992 and 2013 as compared to 1986, no significant difference is seen between the median values of these 2 years. This slight increase in ice thickness could potentially reflect an increase in snow ice formation, as the snow depth globally increased in the last decades and thin (0.05-0.10 m) snow ice is generally found at the surface of

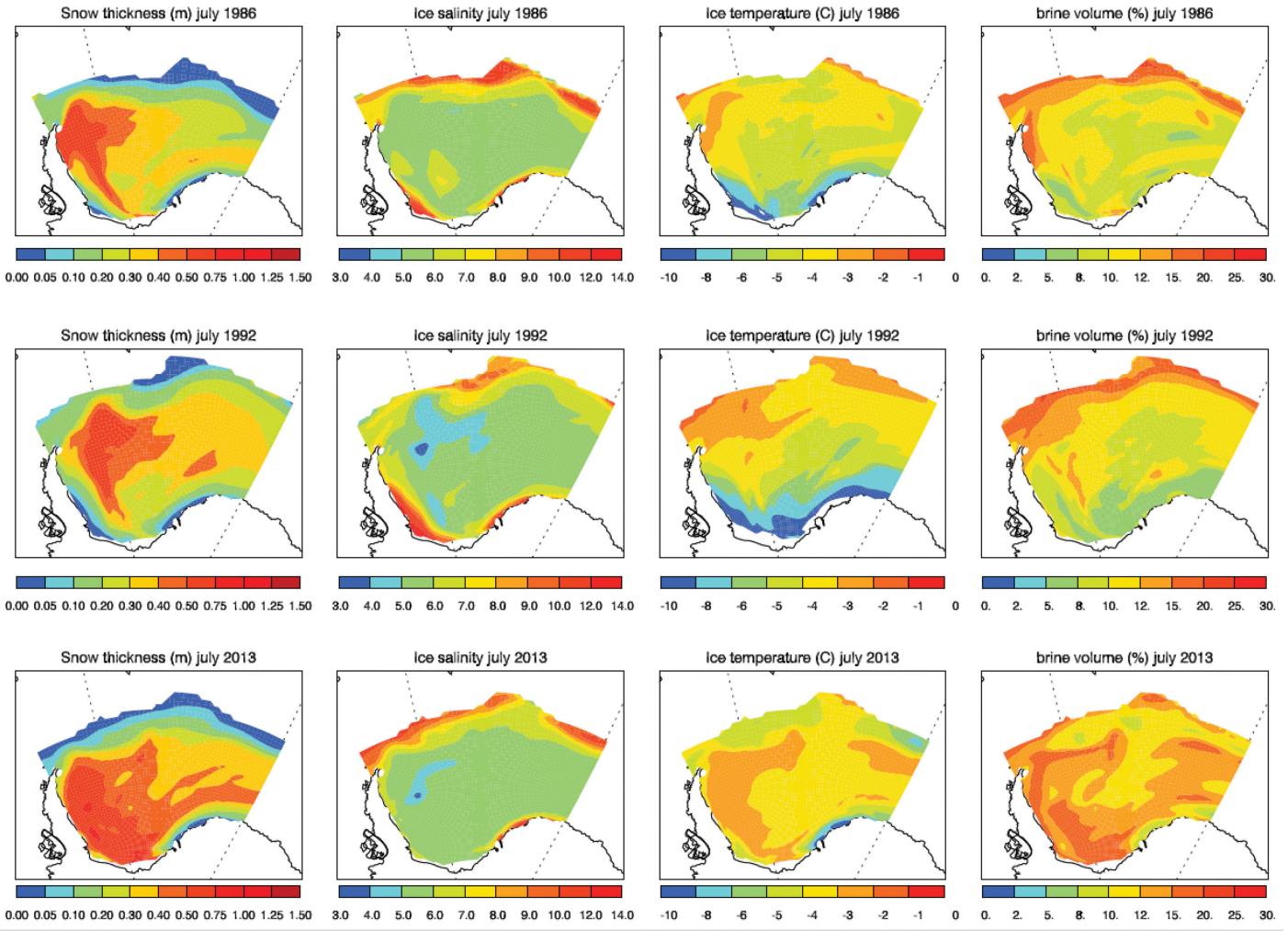

Figure 9. NEMO-LIM3 simulations of Snow thickness/depth, mean bulk ice salinity, mean ice temperature, and mean brine volume in the Weddell Sea for (a) July 1986 (Polarstern Winter Weddell Sea Project 1986), (b) July 1992 (Polarstern ANT X/4), and (c) July 2013 (Polarstern XXIX, AWECS cruise).

the AWECS stations (Figures 3 and 5). Another consequence of the increase in snow depth is the shift of the ice freeboard distribution toward slightly negative values, a global freeboard reduction that was also already present in 1992. This in turn means globally warmer ice (in extreme cases, the ice cover becomes isothermal, as in station 500, Figure 4a), higher brine volumes and more frequent flooding events with the possibility of developing brine tubes in response to a rapidly changing atmospheric environment (cycles of cold and warm synoptic events). Opening of the brine system and triggering of brine movements should favor an extension of photosynthetic activity later in autumn, or even, light-adaptation permitting, in winter. This is what is suggested by the significant increase (Table 1) toward higher Chl-*a* concentration classes (also initiated in 1992), a higher frequency of occurrences of Chl-*a* maxima, as seen in Figure 2d and "spring-like" bottom maxima of Chl-*a* observed at some of the AWECS stations.

At this stage, it is interesting to investigate how well are our observed changes in basic sea ice properties represented in present-day global ocean-sea ice models. Figure 9 shows the results of the simulation with the NEMO-LIM3 model, with "snapshots" of snow depth, mean bulk ice salinity, mean ice temperature, and mean brine volume in the Weddell Sea for July 1986, July 1992, and July 2013. Figure 10 compares the June and July 2013 outputs of the model to the mean ice cover values observed at each station. Snow depth mostly shows values consistent with observations, increasing from negligible at the marginal ice zone to 0.20-0.30 m in the central Weddell Sea. Our cruise track unfortunately did not penetrate the westerly and most southerly part of the Weddell Sea where the model predicts much higher accumulations (Figure 10, left).

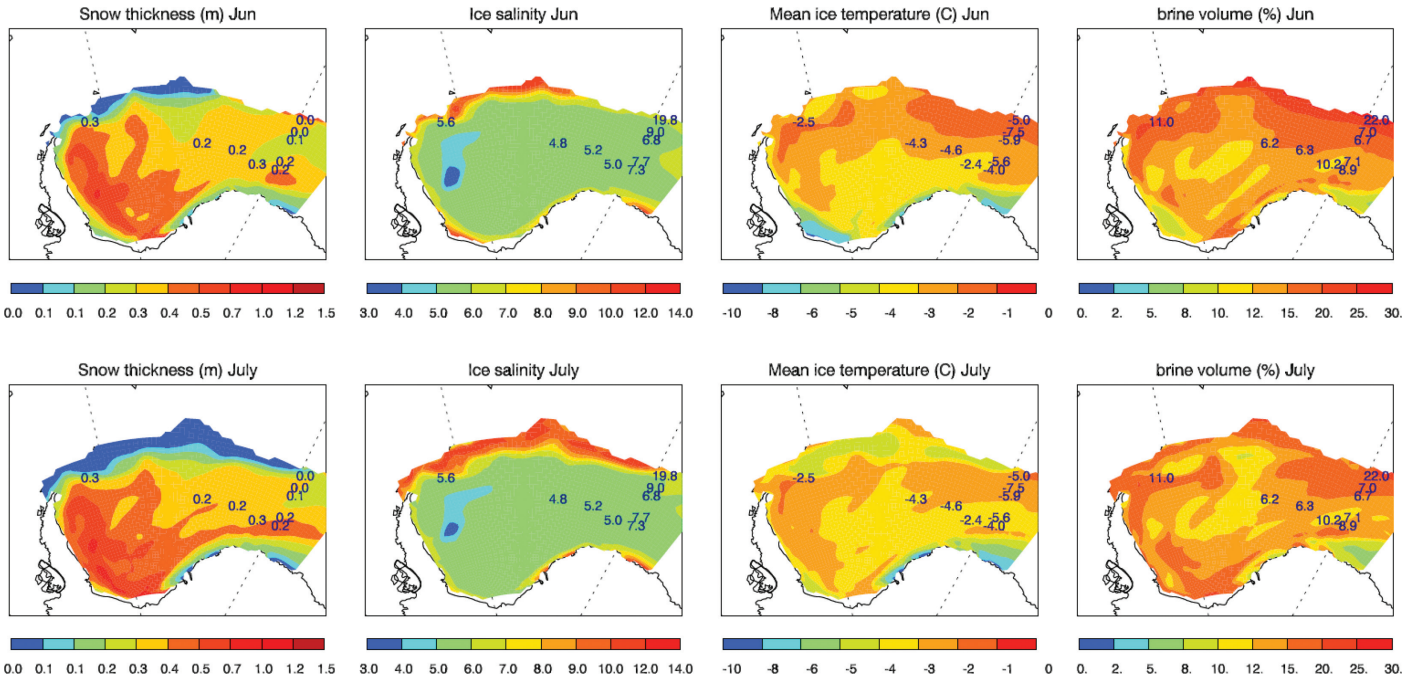

Figure 10. NEMO-LIM3 simulations of snow thickness/depth, mean bulk ice salinity, mean ice temperature, and mean brine volume in the Weddell Sea for July 2013 with observations from the AWECS cruise.

Figure 9 shows an overall increase of snow depth between 1986 and 2013. It is however important to realize that this increase of snow depth is not related to increasing precipitations with time, since the model is forced with monthly climatology of precipitation. Hence, snow can deepen over the years in the model, only because of sea ice processes. Interestingly, Toyota et al. (2016, Figure 12) also provide a reconstruction of $\overline{(P)}-\overline{(E)}$ in the Weddell Sea sector (the area of the present study) between 1990 and 2012, which equally shows no trend. If these reconstructions are correct, other factors than increased precipitation need to be found to explain our 1986–1992–2013 snow depth increase over sea ice (and associated changes in sea ice physics and biogeochemistry) in the Weddell Sea.

Toyota et al. (2016) favored reduced loss of snow in leads and open water, which can indeed occur in the model provided that ice concentration increases with time, which is not clear from model results. We argue that a more efficient contributor is the increasing sea ice season duration. Indeed, as discussed in Stammerjohn et al. (2007, 2012), the Weddell Sea shows a trend of increasing sea ice season duration of about 1–2 d/yr over the 1979–2004 period, which could easily explain an increase of 0.10-0.20 m of snow depth at a net annual precipitation rate of minimum 150 kgm^{-2} (Toyota et al., 2016) over a few decades.

In addition, regardless of the process responsible for the increase in snow thickness in the sea ice model, the increase in snow cover over the years clearly results in an increase in ice temperature and relative brine volume, as observed in our three winters "snapshots" (Figure 9). Observed ice salinities are reasonably well simulated, with an increase at the marginal ice zone, and slight underestimation along the Greenwich meridian. The same is true for the mean ice temperature, which is this time overestimated along the Greenwich meridian. As a result, brine volume is also overestimated. Since the model coherently translates an increase in snow precipitation in a warmer and more permeable ice cover, accordingly to observations, future modeling work should clearly show more interest in attempting to incorporate daily reanalyses of those variables linked with the water cycle (relative humidity, cloudiness, and precipitation).

6. Conclusions

The AWECS winter cruise in June–August 2013 has provided a rare opportunity to document winter sea ice physical and biogeochemical properties in the Weddell Sea. This is of crucial importance in order to assess

the annual budget of the sea ice impact on the climate, through its interactions with the ocean and the atmosphere. Only two previous sea ice-dedicated winter cruises occurred in the Weddell Sea, respectively in 1986 and 1992. These provide a critical reference frame to interpret our new set of data.

It has often been assumed that the sea-ice brine system would evolve toward a closed system in winter, based on the low atmospheric temperatures and low solar radiation, with limited biogeochemical activity and exchanges. Results from both the AWECS cruise and the NEMO-LIM3 model are challenging that view. Sea ice was relatively warm and permeable throughout the study area, for two main reasons: (a) the generalized occurrence of a relatively deep snow cover (a few tens of centimeters) and, (b) large temperature excursions generated by the regular penetration of synoptic events (warm air and heavy snowfalls) all the way to the Antarctic coast. The frequent occurrence of "brine tubes" supports the idea that this alternation of weather regimes combined with heavy snowfall events resulted in a very dynamic brine system, especially in the upper layers of the sea ice cover. Brine tubes are broad linear single feature developing in the top 0.30-0.40 m of sea ice. They differ from typical brine channels by the lack of ramification, larger diameter and straightness. They result from the combination of flooding and temperature cycling in the ice. Temperature cycling translates in the succession of cooling and warming phase. During the cooling phase, surface sea water and brines partly refreeze which increases brine salinity. During the warming phases, these high salinity brines thermodynamically readjust, progressively dissolving the ice as they move downward under gravity.

The impact of such brine tubes on nutrient transport could well be important, combined with the unstable vertical brine density profile, as shown by the higher Rayleigh numbers in some of the stations. This convective process initiated in the upper half of the sea ice cover is more typical of a Spring behavior, as observed during e.g., the 2007 SIMBA cruise in the Bellingshausen Sea (Carnat et al., 2016; Lewis et al., 2011), and contrasts with active thermodynamic sea ice growth generally resulting in elevated Rayleigh numbers in the bottom layers (Notz & Worster, 2009; Zhou et al., 2014b), which was not observed here. Significant snow thicknesses resulted in flooding by sea water at several stations, enhancing the efficiency of the whole process. Occurrences of warm episodes in the surface snow are also witnessed by the co-isotopic signature of the brines, aligning on a mixing line between snow and sea water values.

This dynamic winter brine system appears to have sustained significant Chl-*a* build-up within the sea ice cover (with maximum Chl-*a* levels occurring where brine tubes are observed), primarily as an internal community in the central Weddell Sea. The latter is expected from a sea ice cover generated by a dominant pancake cycle involving scavenging and rafting. Chl-*a* levels increase from the marginal ice zone to the Antarctic coast, suggesting a progressive accumulation through the autumn-winter transition. Repeated measurements at one of the stations after 4 days (Station 506), showed a dramatic increase of the algal community, both in terms of cell numbers and biomass. Although this could have resulted from the patchiness of autotrophic community incorporation and development at an earlier stage of the sea ice cover history, several arguments are suggesting active growth at the time of sampling: compatibility with known cells growth rates for the diatoms community, photosynthetic adaptation to low light levels, bottom Chl-*a* maximum at some stations and, last but not least, constantly low phaeopigments to Chl-*a* ratios for all sea ice samples as opposed to surface sea water values (with global correspondence of Chl-*a* maxima to minimum ratios). This stresses the importance of including "in situ" incubation experiments in future winter sea ice experiments.

Although the number of previous reference winter cruises is obviously too low to describe trends, our results show that the 2013 cruise is characterized by higher snow depth, lower (and more negative) freeboard, and higher Chl-*a* median values compared to the 1986 and 1992 surveys. This result is consistent with the outputs of the NEMO-LIM3 sea ice model, showing a clear trend of increasing snow thickness, mean ice temperature, and mean relative brine volume from 1986 to 2013, and reasonably good agreement with our data set for 2013. Because snowfall is forced from climatology, the increasing trend in snow depth simulated by the model can only be associated with changes in the sea ice state. In addition, Toyota et al. (2016) see no trend in net precipitation in the Weddell Sea for the period of concern, based on ERA-Interim atmospheric reanalysis. Toyota et al. (2016) suggest increasing snow depth, could be associated with reduced loss of snow to open water due to increasing ice concentration. The observed increase in the sea ice season duration (Stammerjohn et al., 2007, 2012) is another efficient means to increase snow depth by catching more snow fall, a mechanism that would be supported by the climate model study of Hezel et al.

(2012) for the future Arctic. A more complete analysis of the simulated snow mass balance, including interannual precipitation forcing, would shed more light on these alternatives.

Clearly, our AWECS data set challenges the traditional assumption that sea ice winter biogeochemical activity is restricted by the very low ambient temperatures and light levels. It suggests that previous estimates of annual budgets of climatically significant gas fluxes across the ocean-sea ice-atmosphere interfaces, essentially based on Spring-Summer observations, will need to also take winter processes into account.

Acknowledgments
The authors wish to warmly thank the Captain and crew of the RV Polarstern and the Chief Scientist Peter Lemke for their unconditional logistic and scientific support during the AWECS cruise. This work is a contribution to the Belgian Science Policy Office project BIGSOUTH (contract SD/CA/05A). The work of SS was funded by the EU 7th Framework project SIDARUS (FP7-SPACE-2010-1, grant agreement 262922). S.M. is supported by the Australian Research Council's Special Research Initiative for Antarctic Gateway Partnership (Project ID SR140300001) and postdoctoral researcher with the FRS-FNRS. D.N. was supported by JSPS KAKENHI grant 12J04175 and 17H04715. The work of C.U. was funded by a Postdoctoral Fellowship of the Université Libre de Bruxelles and the Alfred-Wegener-Institute. The work of A.M.L. was supported by Walter and Andrée de Nottbeck Foundation, Onni Talas Foundation, and Finnish Antarctic Research Program FINNARP. J.J. was supported by the Quantitative Antarctic Science Program jointly led by the University of Tasmania and the Australian Antarctic Division. G.C. benefited from a Belgian Fonds National de la Recherche Scientifique (FRS-FNRS) research grant (contract A 4/5 - MCF/DM - 2657). B.D. is a research associate with the F.R.S-FNRS. Data Base: PANGEA under doi.pangaea.de/10.1594/PANGAEA.834492

References

Arrigo, K. R., Brown, Z. W., & Mills, M. M. (2014). Sea ice algal biomass and physiology in the Amundsen Sea, Antarctica. *Elementa: Science of the Anthropocene*, *2*, 28. https://doi.org/10.12952/journal.elementa.000028

Arrigo, K. R., Dieckmann, D. N., Gosselin, M., Robinson, D. H., Fritsen, C. H., & Sullivan, C. W. (1995). High resolution study of the platelet ice ecosystem in McMurdo Sound, Antarctica: Biomass, nutrient, and production profiles within a dense bloom. *Marine Ecology Progress Series*, *127*, 255–268.

Arrigo, K. R., Mock, T., & Lizotte, M. P. (2010). Primary producers and sea ice. In D. N. Thomas & G. S. Thomas (Eds.), *Sea ice* (p. 621). Oxford, UK: Blackwell Publishing Ltd.

Arrigo, K. R., & Thomas, D. N. (2004). Large scale importance of sea ice biology in the Southern Ocean. *Antarctic Science*, *16*, 471–486. https://doi.org/10.1017/S0954102004002263

Arrigo, K. R., Worthen, D. L., Lizotte, M. P., Dixon, P., & Dieckmann, D. N. (1997). Primary production in Antarctic sea ice. *Science*, *276*(5311), 394–397. https://doi.org/10.1126/science.276.5311.394

Aumont, O., Ethé, C., Tagliabue, A., Bopp, L., & Gehlen, M. (2015). PISCES-v2: An ocean biogeochemical model for carbon and ecosystem studies. *Geoscientific Model Development*, *8*, 2465–2513. https://doi.org/10.5194/gmd-8-2465-2015

Barthélemy, A., Fichefet, T., Goosse, H., & Madec, G. (2015). Modeling the interplay between sea ice formation and the oceanic mixed layer: Limitations of simple brine rejection parameterizations. *Ocean Modelling*, *86*, 141–152. https://doi.org/10.1016/j.ocemod.2014.12.009

Berliand, M. E., & Strokina, T. G. (1980). *Global distribution of the total amount of clouds* (report in Russian, 71 pp.). Hydrometeorology, Leningrad, Russia.

Bluhm, B. A., Gradinger, R. R., & Schnack-Schiel, S. B. (2010). Sea ice meio- and macrofauna. In N. Thomas & G. S. Dieckmann (Eds.), *Sea ice* (p. 621.). Oxford, UK: Blackwell Publishing Ltd.

Bromwich, D. H. (1988). Snowfall in high southern latitudes. *Reviews of Geophysics*, *26*(1), 149–168. https://doi.org/10.1029/RG026i001p00149

Carnat, G., Brabant, F., Dumont, I., Vancoppenolle, M., Ackley, S. F., Fritsen, C., . . . Tison, J. L. (2016). Influence of short-term synoptic events and snow depth on DMS, DMSP, and DMSO dynamics in Antarctic spring sea ice. *Elementa*, *4*, 000135. https://doi.org/10.12952/journal.elementa.000135

Carnat, G., Papakyriakou, T. N., Geilfus, N. X., Brabant, F., Delille, B., Vancoppenolle, M., . . . Tison, J. L. (2013). Investigations on physical and textural properties of Arctic first-year sea ice in the Amundsen Gulf, Canada, November 2007-June 2008 (IPY-CFL system study). *Journal of Glaciology*, *59*(217), 819–837. https://doi.org/10.3189/2013JoG12J148

Cox, G. F. N., & Weeks, W. F. (1983). Equations for determining the gas and brine volumes in sea-ice samples. *Journal of Glaciology*, *29*(102), 306–316.

Dai, A., & Trenberth, K. E. (2002). Estimates of freshwater discharge from continents: Latitudinal and seasonal variations. *Journal of Hydrometeorology*, *3*, 660–686.

Delille, B. (2006). *Inorganic carbon dynamics and air-ice-sea CO_2 fluxes in the open and coastal waters of the Southern Ocean* (PhD thesis), Liège, Belgium: Université de Liège.

Delille, B. Vancoppenolle, M., Geilfus, N.-X., Tilbrook, B., Lannuzel, D., V. Schoemann, . . . Tison, J.-L. (2014). Southern Ocean CO_2 sink: The contribution of the sea ice. *Journal of Geophysical Research: Oceans*, *119*, 6340–6355. https://doi.org/10.1002/2014JC009941

Dieckmann, G. S., & Hellmer, H. H. (2010). The importance of sea ice: An Overview. In D. N. Thomas & G. S. Dieckmann (Eds.) *Sea ice* (p. 621). Oxford, UK: Blackwell Publishing Ltd.

Eicken, H. (1998). Deriving modes and rates of ice growth in the Weddell Sea from microstructural, salinity and stable-isotope data. In M. O. Jeffries (Ed.), *Antarctic sea ice: Physical processes, interactions and variability* (Vol. 74, pp. 89–122). Washington, DC: American Geophysical Union. https://doi.org/10.1029/AR074p0089

Eicken, H., Grenfell, T. C., Perovich, D. K., Richter-Menge, J. A., & Frey, K. (2004). Hydraulic controls of summer Arctic pack ice albedo. *Journal of Geophysical Research*, *109*, C08007. https://doi.org/10.1029/2003JC001989

Eicken, H., Lange, M. A., & Dieckmann, D. N. (1991). Spatial variability of sea-ice properties in the Northwestern Weddell Sea. *Journal of Geophysical Research*, *96*(C6), 10603–10615.

Else, B. G. T., Papakyriakou, T. N., Galley, R. J., Drennan, W. M., Miller, L. A., & Thomas, H. (2011). Wintertime CO_2 fluxes in an Arctic polynya using eddy covariance: Evidence for enhanced air-sea gas transfer during ice formation. *Journal of Geophysical Research*, *116*, C00G03. https://doi.org/10.1029/2010JC006760

Evans, C. A., O'reilly, J. E., O'reilly, J. E., & Thomas, J. P. and BIOMASS. (1987). *A handboook for the measurement of chlorophyll a and primary production*. College Station, TX: Texas A&M University.

Fetterer, F., Knowles, K., Meier, W., Savoie, M., & Windnagel, A. K. (2016). *Sea ice index*, version 2. Boulder CO: National Snow and Ice Data Center (NSIDC). https://doi.org/10.7265/N5736NV7

Flores, H. Atkinson, A., Kawaguchi, S., Krafft, B. A., Milinevsky, G., Nicol, S., . . . Werner, T. (2012). Impact of climate change on Antarctic krill. *Marine Ecology Progress Series*, *458*, 1–19. https://doi.org/10.3354/meps09831

Fofonoff, N. P. (1985). Physical properties of seawater: A new salinity scale and equation of state for seawater. *Journal of Geophysical Research*, *90*(C2), 3332–3342.

Freitag, J. (1999). Untersuchungen zur Hydrologie des arktischen Meereises-Konsequenzen für den kleinskaligen Stofftransport, *Berichte zur Polarforschung/Reports on Polar Research*, *325*, 150 pp.

Garrison, D. L., Ackley, S. F., & Buck, K. R. (1983). A physical mechanism for establishing algal population in frazil ice. *Nature*, *306*, 363–365.

Garrison, D. L., & Buck, K. R. (1986). Organism losses during ice melting: A serious bias in sea ice community studies. *Polar Biology*, *6*(4), 237–239.

Golden, K. M. (2003). Critical behavior of transport in sea ice. *Physica B*, *338*(1–4), 274–283. https://doi.org/10.1016/j.physb.2003.08.007

Golden, K. M., Ackley, S. F., & Lytle, V. (1998). The percolation phase transition in sea ice. *Science*, *282*, 2238–2240.
Gosselin, M., Legendre, L., Therriault, J.-C., & Demers, S. (1990). Light and nutrient limitation on sea-ice microalgae (Hudson Bay, Canadian Arctic). *Journal of Phycology*, *26*, 220–232.
Gradinger, R. R., & Ikävalko, J. (1998). Organism incorporation into newly forming Arctic sea ice in the Greenland Sea. *Journal of Phytoplankton Research*, *20*(5), 871–886.
Grimm, R., Notz, D., Glud, R. N., Rysgaard, S., & Six, K. (2016). Assesment of the sea -ice carbon pump: Insights from a three-dimensional ocean-sea-ice biogeochemical model (MPIOM/HAMOCC). *Elementa*, *4*, 000136. https://doi.org/10.12952/journal.elementa.000136
Guillard, R. R. L. (1973). Division rates. In J. R. Stein (Ed.), *Handbook of phycological methods: Culture methods and growth measurements*. Cambridge, UK: Cambridge University Press.
Heinesch, B., Yernaux, M., Aubinet, M., Geilfus, N. X., Papakyriakou, T. N., Carnat, G., . . . Delille, B. (2009). Measuring Air-ice CO_2 fluxes in the Arctic, *FluxLetter, the Newsletter of FLUXNET*, 2, 9–10.
Hezel, P. J., Zhang, X., Bitz, C. M., Kelly, B. P., & Massonnet, F. (2012). Projected decline in spring snow depth on Arctic sea ice caused by progressively later autumn open ocean freeze-up this century. *Geophysical Research Letters*, *39*, L17505. https://doi.org/10.1029/2012GL052794
Horner, R. A., Ackley, S. F., Dieckmann, G. S., Gulliksen, B., Hoshiai, T., Legengre, L., . . . Sullivan, C. W. (1992). Ecology of sea ice biota: 1. Habitat, terminology, and methodology. *Polar Biology*, *12*, 417–427.
Hunke, E. C., Notz, D., Turner, A. K., & Vancoppenolle, M. (2011). The multiphase physics of sea ice: A review for model developers. *The Cryosphere*, *5*(4), 989–1009. https://doi.org/10.5194/tc-5-989-2011
Jeffries, M. O., Shaw, R. A., Morris, K., Veazey, A. L., & Krouse, H. R. (1994). Crystal structure, stable isotopes ($d^{18}O$) and development of sea ice in the Ross, Amundsen and Bellingshausen Seas, Antarctica. *Journal of Geophysical Research*, *99*(C1), 985–995.
Jeffries, M. O., Worby, A. P., Morris, K., & Weeks, W. F. (1997). Seasonal variations in the properties and structural composition of sea ice and snow cover in the Bellingshausen and Amundsen Seas, Antarctica. *Journal of Glaciology*, *43*(143), 138–151.
Jouzel, J., & Souchez, R. (1982). Melting-refreezing at the glacier sole and the isotopic composition of the ice. *Journal of Glaciology*, *28*(98), 35–42.
Kalnay, E., Kanamitsu, M., Kistler, R., Collins, W., Deaven, D., Gandin, L., . . . Joseph, D. (1996). The NCEP/NCAR 40-year reanalysis project. *Bulletin of the American Meteorological Society*, *77*(3), 437–471. https://doi.org/10.1175/1520-0477(1996)077<0437:TNYRP>2.0.CO;2
Kottmeier, S. T., Grossi, S. M., & Sullivan, C. W. (1987). Sea ice microbial communities (SIMCO).VIII. Bacterial production in the annual sea ice of Mc Murdo Sound, Antarctica. *Marine Ecology Progress Series*, *35*, 175–186.
Krembs, C., Eicken, H., & Deming, J. W. (2011). Exopolymer alteration of physical properties of sea ice and implications for ice habitability and biogeochemistry in a warmer Arctic. *Proceedings of National Academy of Sciences of the United States of America*, *108*, 3653–3658. https://doi.org/10.1073/pnas.1100701108
Lange, M. A. (1988). Basic properties of Antarctic sea ice as revealed by textural analysis of ice cores. *Annals of Glaciology*, *10*, 95–101.
Lange, M. A. (1990). Development and physical properties of sea ice in the Weddell Sea, Antarctica. In *Sea ice properties and processes* (Monogr. Rep. 90-1, 22–40 pp.). Hanover, NH: CRREL.
Lange, M. A., Ackley, S. F., Wadhams, P., Dieckmann, G. S., & Eicken, H. (1989). Development of sea ice in the Weddell Sea, Antarctica. *Annals of Glaciology*, *12*, 92–96.
Lange, M. A., Schlosser, P., Ackley, S. F., Wadhams, P., & Dieckmann, G. S. (1990). ^{18}O concentrations in sea ice of the Weddell Sea, Antarctica. *Journal of Glaciology*, *36*(124), 315–323.
Langway, C. C. J. (1958). *Ice fabrics and the Universal stage* (Tech. Rep. 62, 16 pp.). Hanover, NH: CRREL.
Lannuzel, D., De Jong, J., Schoemann, V., Trevena, A., Tison, J.-L., & Chou, L. (2006). Development of a sampling and flow injection analysis technique for iron determination in the sea ice environment. *Analytica Chimica Acta*, *556*(2), 476–483.
Large, W. G., & Yeager, S. G. (2004). *Diurnal to decadal global forcing for ocean and sea ice models: The data sets and flux climatologies* (report, 112 pp.). Boulder, CO: National Center for Atmospheric Research.
Lenaerts, J. T. M., Vizcaino, M., Fyke, J., van Kampenhout, L., & van den Broeke, M. R. (2016). Present-day and future Antarctic ice sheet climate and surface mass balance in the Community Earth System Model. *Climate Dynamics*, *47*(5), 1367–1381. https://doi.org/10.1007/s00382-015-2907-4
Leonard, K. C., & Maksym, T. (2011). The importance of wind-blown snow redistribution to snow accumulation on Bellingshausen Sea ice. *Annals of Glaciology*, *52*(57), 271–278. https://doi.org/10.3189/172756411795931651
Lepparänta, M., & Manninen, T. (1988). *The brine and gas content of sea ice with attention to low salinities and high temperatures* (Int. Rep. 88-2, 15 pp.). Helsinki, Finland: Finnish Institute Marine Research.
Leu, E., Søreide, J. E., Hessen, D. O., Falk-Petersen, S., & Berge, J. (2011). Consequences of changing sea-ice cover for primary and secondary producers in the European Arctic shelf seas: Timing, quantity, and quality. *Progress in Oceanography*, *90*(1–4), 18–32. https://doi.org/10.1016/j.pocean.2011.02.004
Lewis, M. J., Tison, J.-L., Weissling, B., Delille, B., Ackley, S., Brabant, F., & Xie, H. (2011). Sea ice and snow cover characteristics during the winter-spring transition in the Bellingshausen Sea: An overview of SIMBA 2007. *Deep Sea Research Part II: Topical Studies in Oceanography*, *58*(9), 1019–1038.
Lizotte, M. P. (2001). The contributions of sea ice algae to Antarctic marine primary production. *American Zoologist*, *41*(1), 57–73. https://doi.org/10.1668/0003-1569(2001)041[0057:TCOSIA]2.0.CO;2
Loose, B., McGillis, W. R., Perovich, D., Zappa, C. J., & Schlosser, P. (2013). A parameter model of gas exchange for the seasonal sea ice zone. *Ocean Science Discussions*, *10*, 1169–1204.
Loose, B., & Schlosser, P. (2011). Sea ice and its effect on CO_2 flux between the atmosphere and the Southern Ocean interior. *Journal of Geophysical Research*, *116*, C11019. https://doi.org/10.1029/2010JC006509
Lovely, A., Loose, B., Schlosser, P., McGillis, W., Zappa, C., Perovich, D., . . . Friedrich, R. (2015). The gas transfer through polar sea ice experiment: Insights into the rates and pathways that determine geochemical fluxes. *Journal of Geophysical Research: Oceans*, *120*, 8177–8194. https://doi.org/10.1002/2014JC010607
Madec, G., and NEMO-Team (2016). *NEMO Ocean Engine version 3.6 stable* (Rep. 1288–1619, 406 pp.). Paris, France: Institut Pierre-Simon Laplace.
Meiners, K. M., Vancoppenolle, M., Thanassekos, S., Dieckmann, G. S., Thomas, D. N., Tison, J.-L., . . . Raymond, B. (2012). Chlorophyll a in Antarctic sea ice from historical ice core data. *Geophysical Research Letters*, *39*, L21602. https://doi.org/10.1029/2012GL053478
Menden-Deuer, S., & Lessard, E. J. (2000). Carbon to volume relationships for dinoflagellates, diatoms and other protist plankton. *Limnology and Oceanography*, *45*(3), 569–579.
Meyer, H., Schönicke, L., Wand, U., Hubberten, H.-W., & Friedrichsen, H. (2000). Isotope studies of hydrogen and oxygen in ground ice? Experiences with the equilibration technique. *Isotopes in Environmental and Health Studies*, *36*, 133–149.
Miller, L. A., Papakyriakou, T. N., Collins, R. E., Deming, J. W., Ehn, J. K., Macdonald, R. W., . . . Sutherland, N. (2011). Carbon dynamics in sea ice: A winter flux time series. *Journal of Geophysical Research*, *116*, C02028. https://doi.org/10.1029/2009JC006058

Mock, T. (2002). In situ primary production in young Antartic sea ice. *Hydrobiologia*, *470*, 127–132.
Mock, T., & Gradinger, R. R. (1999). Determination of Arctic ice algal production with a new in situ incubation technique. *Marine Ecology Progress Series*, *177*, 15–26.
Mock, T., Meiners, K. M., & Giesenhagen, H. C. (1997). Bacteria in sea ice and underlying brackish water at 54°26′50″N (Baltic Sea, Kiel Bight). *Marine Ecology Progress Series*, *158*, 23–40.
Moreau, S., Vancoppenolle, M., Bopp, L., Aumont, O., Madec, G., Delille, B., . . . Goosse, H. (2016). Assesment of the sea-ice carbon pump: Insights from a three-dimensional ocean-sea-ice biogeochemical model (NEMO-LIM-PISCES). *Elementa*, *4*, 000122. https://doi.org/10.12952/journal.elementa.000122
Moreau, S., Vancoppenolle, M., Delille, B., Tison, J.-L., Zhou, J., Kotovitch, M., . . . Goosse, H. (2015). Drivers of inorganic carbon dynamics in first-year sea ice: A model study. *Journal of Geophysical Research: Oceans*, *120*, 471–495. https://doi.org/10.1002/2014JC010388
Mundy, C. J., Barber, D. G., & Michel, C. (2005). Variability of snow and ice thermal, physical and optical properties pertinent to sea ice algae biomass during Spring. *Journal of Marine Systems*, *58*, 107–120.
Niemi, M., Kuparinen, J., & Uusi-Rauva, A. (1983). Preparation of ^{14}C-labeled algal samples for liquid scintillation counting. *Hydrobiologia*, *106*, 149–156.
Notz, D., & Worster, M. G. (2008). In situ measurements of the evolution of young sea ice. *Journal of Geophysical Research*, *113*, C03001. https://doi.org/10.1029/2007JC004333
Notz, D., & Worster, M. G. (2009). Desalination processes of sea ice revisited. *Journal of Geophysical Research*, *114*, C05006. https://doi.org/10.1029/2008JC004885
Olenina, I., Hadju, S., Edler, L., Andersson, A., Wasmund, N., Busch, S., . . . Niemkiewicz, E. (2006). Biovolumes and size-classes of phytoplankton in the Baltic Sea. In *HELCOM Baltic Sea Environment Proceedings* (Vol. 106, pp. 1–144).
Papakyriakou, T. N., & Miller, L. A. (2011). Springtime CO_2 exchange over seasonal sea ice in the Canadian Arctic Archipelago. *Annals of Glaciology*, *52*(57), 215–224. https://doi.org/10.3189/172756411795931534
Petrich, C., & Eicken, H. (2017). Overview of sea ice growth and properties. In D. N. Thomas (Ed.), *Sea ice* (p. 652). Chichester, UK: John Wiley.
Philippe, M., Tison, J.-L., Fjøsne, K., Hubbard, B., Kjær, H. A., Lenaerts, J. T. M., . . . Pattyn, F. (2016). Ice core evidence for a 20th century increase in surface mass balance in coastal Dronning Maud Land, East Antarctica. *The Cryosphere*, *10*(5), 2501–2516. https://doi.org/10.5194/tc-10-2501-2016
Platt, T., Gallegos, C. L., & Harrison, W. G. (1980). Photoinhibition of photosynthesis in natural assemblages of marine phytoplancton. *Journal of Marine Research*, *38*, 687–701.
Pringle, D., & Ingham, M. (2009). Measuring sea ice thermal, electrical and hydraulic properties and processes. In H. Eicken ET AL. (Eds.) *Field techniques for sea ice research* (p. 592). Fairbanks, AK: University of Alaska Press.
Rintala, J. M., Piiparinen, J., Blomster, J., Majaneva, M., Müller, S., Uusikivi, J., & Autio, R. (2014). Fast direct melting of brackish sea-ice samples results in biologically more accurate results than slow buffered melting. *Polar Biology*, *37*, 1811–1822. https://doi.org/10.1007/s00300-014-1563-1
Rousset, C., Vancoppenolle, M., Madec, G., Fichefet, T., Flavoni, S., Barthélemy, A., . . . Vivier, F. (2015). The Louvain-La -Neuve sea ice model LIM 3.6: Global and regional capabilities. *Geoscientific Model Development*, *8*, 2991–3005. https://doi.org/10.5194/gmd-8-2991-2015
Rysgaard, S., Bendtsen, J., Delille, B., Dieckmann, G. S., Glud, R. N., Kennedy, H., . . . Tison, J.-L. (2011). Sea ice contribution to the air–sea CO_2 exchange in the Arctic and Southern Oceans. *Tellus, Series B*, *63*(5), 823–830. https://doi.org/10.1111/j.1600-0889.2011.00571.x
Sievers, J., L.L, S., Papakyriakou, T. N., Else, B. G. T., Sejr, M. K., Haubjerg Søgaard, D., Barber, D. G., & Rysgaard, S. (2015). Winter observations of CO_2 exchange between sea ice an the atmosphere in a coastal fjord environment. *The Cryosphere*, *9*, 1701–1713. https://doi.org/10.5194/tc-9-1701-2015
Smetacek, V., Scharek, R., Gordon, L. I., Eicken, H., Fahrbach, E., Rohardt, G., & Moore, S. (1992). Early spring phytoplankton blooms in ice platelet layers of the southern Weddell Sea, Antarctica. *Deep Sea Research Part A. Oceanographic Research Papers*, *39*(2), 153–168. https://doi.org/10.1016/0198-0149(92)90102-Y
Smith, R. E. H., & Herman, A. W. (1991). Productivity of sea ice algae: In situ vs. incubator methods. *Journal of Marine Systems*, *2*(1–2), 97–110.
Smith, W. O., & Nelson, D. M. (1986). Importance of ice edge phytoplankton blooms in the Southern Ocean. *BioSciences*, *36*, 251–257.
Song, H. J., Lee, J. H., Kim, G. W., Ahn, S. H., Joo, H.-M., Jeong, J. Y., Yang, E. J., . . . Lee, S. H. (2016). In-situ measured primary productivity of ice algae in Arctic sea ice floes using a new incubation method. *Ocean Science Journal*, *51*(3), 387–396. https://doi.org/10.1007/s12601-016-0035-7
Sørensen, L. L., Jensen, B., Glud, R. N., McGinnis, D. F., Sejr, M. K., Sievers, J., . . . Rysgaard, S. (2014). Parameterization of atmosphere–surface exchange of CO_2 over sea ice. *The Cryosphere*, *8*(3), 853–866. https://doi.org/10.5194/tc-8-853-2014
Souchez, R., & Jouzel, J. (1984). On the isotopic composition in dD and d^{18}O of water and ice during freezing. *Journal of Glaciology*, *30*(106), 369–372.
Souchez, R., Tison, J.-L., & Jouzel, J. (1987). Freezing rate determination by the isotopic composition of the ice. *Geophysical Research Letters*, *14*(6), 599–602.
Souchez, R., Tison, J.-L., & Jouzel, J. (1988). Deuterium concentration and growth rate of Antarctic first-year sea ice. *Geophysical Research Letters*, *15*(12), 1385–1388.
Stammerjohn, S. E., Martinson, D. G., Smith, R. C., Yuan, X., & Rind, D. (2007). Trends in Antarctic annual sea ice retreat and advance and their relation to El-Nino-Southern Oscillation and Southern Annular Mode variability. *Journal of Geophysical Research*, *113*, C03S90. https://doi.org/10.1029/2007JC004269
Stammerjohn, S. E., Massom, R., Rind, D., & Martinson, D. G. (2012). Regions of rapid sea ice change: An inter-hemispheric seasonal comparison. *Geophysical Research Letters*, *39*, L06501. https://doi.org/10.1029/2012GL050874
Steemann Nielsen, E. (1952). *The use of radioactive carbon (^{14}C) for measuring organic production in the sea* (report, 117–140 pp.). Copenhagen, Denmark: Conseil Permanent International pour l'Exploration de la Mer.
Steiner, N. S., Lee, W. G., & Christian, J. R. (2013). Enhanced gas fluxes in small sea ice leads and cracks: Effects on CO_2 exchange and ocean acidification. *Journal of Geophysical Research: Oceans*, *118*, 1195–1205. https://doi.org/10.1002/jgrc.20100
Sturm, M., & Massom, R. A. (2017). Snow in the sea ice system: Friend or foe?. In D. N. Thomas & G. S. Dieckmann (Ed.) *Sea ice* (p. 652). Chichester, UK: John Wiley.
Thomas, D. N., & Dieckmann, G. S. (2002). Antarctic sea ice–a habitat for extremophiles. *Science*, *295*(5555), 641–644.
Thomas, D. N., Papadimitriou, S., & Michel, C. (2010). Biogeochemistry of sea ice. In D. N. Thomas & G. S. Dieckmann (Eds.), *Sea ice* (p. 621). Oxford, UK: Blackwell Publishing Ltd.

Tison, J. L., Haas, M. M., Gowing, S., Sleewaegen, S., & Bernard, A. (2002). Tank study of physico-chemical controls on gas content and composition during growth of young sea ice. *Journal of Glaciology*, *48*(161), 177–191.

Toyota, T., Massom, R., Lecomte, O., Nomura, D., Heil, P., Tamura, T., & Fraser, A. D. (2016). On the extraordinary snow on the sea ice off East Antarctica in late winter, 2012. *Deep Sea Research Part II: Topical Studies in Oceanography*, *131*, 53–67. https://doi.org/10.1016/j.dsr2.2016.02.003

Trenberth, K. E., Olson, J. G., & Large, W. G. (1989). *A global ocean wind stress climatology based on ECMWF analyses* (NCAR Technical Note - NCAR/TN-338 + STR, 93 pp.). Boulder, CO: National Center for Atmospheric Research.

Ütermöhl, H. (1958). Zur Vervollkommnung der quantitativen Phytoplankton-Methodik. Mitteilungen Internationale Vereinigung für Theoretische und Angewandte. *Limnologie*, *9*, 1–38.

Vancoppenolle, M., Fichefet, T., Goosse, H., Bouillon, S., Madec, G., & Maqueda, M. A. M. (2009). Simulating the mass balance and salinity of Arctic and Antarctic sea ice. 1. Model description and validation. *Ocean Modelling*, *27*(1–2), 33–53. https://doi.org/10.1016/j.ocemod.2008.10.005

Vancoppenolle, M., Meiners, K. M., Michel, C., Bopp, L., Brabant, F., Carnat, G., . . . P. van der Merwe (2013). Role of sea ice in global biogeochemical cycles: Emerging views and challenges. *Quaternary Science Reviews*, *79*, 207–230. https://doi.org/10.1016/j.quascirev.2013.04.011

Vancoppenolle, M., & Tedesco, L. (2017). Numerical models of sea ice biogeochemistry. In D. N. Thomas & G. S. Dieckmann (Eds.), *Sea ice* (p. 652). Chichester, UK: John Wiley.

Wood, A. M., Everroad, R. C., & Wingard, L. M. (2005). Measuring growth rates in microalgal cultures. In R. A. Anderson (Ed.), *Algal culturing techniques* (pp. 269–285). Burlington, NJ: Elsevier Academic Press.

Worby, A., Massom, Allison, R. I., Lytle, V. I., & Heil, P. (1998). East Antarcric sea ice: A review of its structure, properties and drift. In M. O. Jeffries (Ed.), *Antarctic sea ice: Physical processes, interactions and variability* (p. 407). Washington DC: American Geophysical Union

Zemmelink, H. J., Delille, B., Tison, J. L., Hintsa, E. J., Houghton, L., & Dacey, J. W. H. (2006). CO_2 deposition over the multi-year ice of the western Weddell Sea. *Geophysical Research Letters*, *33*, L13606. https://doi.org/10.1029/2006GL026320

Zhou, J., Delille, B., Brabant, F., & Tison, J. L. (2014a). Insights into oxygen transport and net community production in sea ice from oxygen, nitrogen and argon concentrations. *Biogeosciences*, *11*, 5007–5020. https://doi.org/10.5194/bg-11-5007-2014

Zhou, J., Delille, B., Eicken, H., Vancoppenolle, M., Brabant, F., Carnat, G., . . . Tison, J. L. (2013). Physical and biogeochemical properties in landfast sea ice (Barrow, Alaska): Insights on brine and gas dynamics across seasons. *Journal of Geophysical Research: Oceans*, *118*, 3172–3189. https://doi.org/10.1002/jgrc.20232

Zhou, J., Delille, B., Kaartokallio, H., Kattner, G., Kuosa, H., Tison, J.-L., . . . Thomas, T. N.(2014b). Physical and bacterial controls on inorganic nutrients and dissolved organic carbon during a sea ice growth and decay experiment. *Marine Chemistry*, *166*, 59–69. https://doi.org/10.1016/j.marchem.2014.09.013

Erratum

In the originally published version of this article, the name of co-author S. Hendricks was misspelled. This has since been corrected and this version may be considered the authoritative version of record.